environments

Article

Integrated Surface and Tropospheric Column Analysis of Sulfur Dioxide Variability at the Lamezia Terme WMO/GAW Regional Station in Calabria, Southern Italy

Francesco D'Amico [1,2,*], Teresa Lo Feudo [1,*], Daniel Gullì [1], Ivano Ammoscato [1], Mariafrancesca De Pino [1], Luana Malacaria [1], Salvatore Sinopoli [1], Giorgia De Benedetto [1] and Claudia Roberta Calidonna [1,*]

[1] Institute of Atmospheric Sciences and Climate, National Research Council of Italy, Area Industriale Comp. 15, 88046 Lamezia Terme, Catanzaro, Italy; d.gulli@isac.cnr.it (D.G.); i.ammoscato@isac.cnr.it (I.A.); m.depino@isac.cnr.it (M.D.P.); l.malacaria@isac.cnr.it (L.M.); s.sinopoli@isac.cnr.it (S.S.); g.debenedetto@isac.cnr.it (G.D.B.)

[2] Department of Biology, Ecology and Earth Sciences, University of Calabria, Via Bucci Cubo 15B, 87036 Rende, Cosenza, Italy

* Correspondence: f.damico@isac.cnr.it or francesco.damico@unical.it (F.D.); t.lofeudo@isac.cnr.it (T.L.F.); claudiaroberta.calidonna@cnr.it (C.R.C.)

Abstract: Sulfur dioxide (SO_2) can be of natural and anthropogenic origin and is one of the sulfur compounds present in the atmosphere. Among natural sources, volcanoes contribute with relevant annual outputs, and major eruptions lead to spikes in these outputs. In the case of anthropogenic pollution, SO_2 emissions are mostly correlated with the sulfur content of fuels, which has been the focus of specific emission mitigation policies for decades. Following other examples of cyclic and multi-year evaluations, an analysis of SO_2 at the Lamezia Terme (code: LMT) WMO/GAW (World Meteorological Organization—Global Atmosphere Watch) station in Calabria, Southern Italy, was performed. The coastal site is characterized by wind circulation patterns that result in the detection of air masses with low or enhanced anthropic influences. The presence of the Aeolian Arc of active, quiescent, and extinct volcanoes, as well as Mount Etna in Sicily, may influence LMT observations with diffused SO_2 emissions. For the first time in the history of the LMT, a multi-year analysis of a parameter has been integrated with TROPOMI data gathered by Sentinel-5P and used to test total tropospheric column densities at the LMT itself and select coordinates in the Tyrrhenian and Ionian seas. Surface and satellite data indicate that SO_2 peaks at the LMT are generally linked to winds from the western–seaside wind corridor, a pattern that is compatible with active volcanism in the Tyrrhenian Sea and maritime shipping to and from the Gioia Tauro port located in the same region. The findings of this research provide the basis for enhanced source apportionment, which could further differentiate anthropogenic sources in the area from natural outputs.

Keywords: sulfur dioxide; GAW; Lamezia Terme; Mediterranean basin; Tyrrhenian Sea; Ionian Sea; surface measurements; TROPOMI; tropospheric column data

Academic Editors: Yonghang Lai and Peter Brimblecombe

Received: 26 November 2024
Revised: 12 January 2025
Accepted: 14 January 2025
Published: 16 January 2025

Citation: D'Amico, F.; Lo Feudo, T.; Gullì, D.; Ammoscato, I.; De Pino, M.; Malacaria, L.; Sinopoli, S.; De Benedetto, G.; Calidonna, C.R. Integrated Surface and Tropospheric Column Analysis of Sulfur Dioxide Variability at the Lamezia Terme WMO/GAW Regional Station in Calabria, Southern Italy. *Environments* **2025**, *12*, 27. https://doi.org/10.3390/environments12010027

1. Introduction

Sulfur dioxide (SO_2), sometimes spelled as sulphur dioxide, is one of the sulfur compounds present in the atmosphere and can be natural or anthropogenic in origin [1–4].

Among natural sources of SO_2, volcanoes contribute a significant emission rate [5–8]. The direct impact of volcanic eruptions on SO_2 concentrations in the troposphere and the stratosphere has been documented in the past few decades [9–12]. The Mt. Pinatubo

eruption of June 1991 set a milestone in the implementation of plume-tracking technologies, satellite data, airborne measurements, and global collaborative networks used to monitor SO_2 emissions from the volcano and the consequent diffusion [13–17]. The Hunga Tonga–Hunga Ha'apai eruption of 2022, which is considered the most explosive eruption of the past 140 years, resulted in significant SO_2 output that was promptly tracked with multiple methodologies [18,19].

Wildfires, agricultural fires, and other forms of biomass burning also result in SO_2 emissions, as well as the release of other sulfur compounds, which influence the overall budget on a global scale [20–25]. Volcanic and wildfire emissions of SO_2 have a direct impact on the atmosphere's ERF (effective radiative forcing), in conjunction with aerosols; for this reason, SO_2 is also the subject of evaluations meant for assessing the climate change potential [26–28].

Anthropogenic emissions are primarily due to fossil fuels and their sulfur content, whose impact on the environment does not affect all areas of the globe via the same mechanisms [29]. Vehicular traffic has been a major source of anthropogenic SO_2, and regulations—in addition to new technologies—have led to the implementation of low-sulfur fuels, which reduce the output from vehicles [30–33]. The oil and gas sector is also linked to SO_2 emissions at various stages [34]. Emissions from this sector are such that they pose a health hazard for workers operating in the field of oil and gas [35].

Shipping is among the main sources of anthropogenic SO_2 [36–38], and air quality parameters in areas where ports are present are known to be affected by maritime traffic [39]. In the Mediterranean, the Suez Canal is a major hotspot for such activities, and a comparative study between standard pollution levels and the levels during periods of exceptionally low traffic, such as during the COVID-19 pandemic and the *Ever Given* incident, showed relevant reductions in SO_2 levels [40]. In the past few years, new technologies have been implemented in the effort to model [41], and also mitigate [42], SO_2 emissions related to maritime traffic. The use of low-sulfur fuel in maritime shipping can effectively reduce the degrees of pollution [43,44]. Aviation fuel is also affected by similar issues [45–47], and the physical–chemical processes that occur at high altitudes in exhaust plumes have been the focus of scientific research meant to assess the extent of aviation fuel-related pollution [48]. Most SO_2 emissions related to aviation occur during the cruise phase and therefore have an impact over wide regions in a short amount of time [49]. Many techniques have been tested to provide accurate information on the impact of aircraft engine exhausts on the total budget of anthropogenic emissions [50,51]. With the rise in SAF (sustainable aviation fuel), sulfur content has been reduced, and the impacts of such emissions on the environment are partially mitigated [52].

As a pollutant, SO_2 is short-lived: depending on a number of environmental factors, its persistence in the atmosphere may be limited to two days [53–56]. In the atmosphere, chemical reactions between SO_2 and other compounds occur [57]: following the reaction with water droplets, sulfuric acid (H_2SO_4)—which is responsible for the acid rain phenomenon—is released [58].

The effects of SO_2 on human health are well documented [59]. SO_2 affects the respiratory system [60] and also poses mental health concerns [61,62]. Globally, it causes more than one million premature deaths every year [63] and prolonged exposure can negatively affect pregnancies [64–67].

The adverse effects of SO_2 have led to global mitigation policies that have managed to reduce the annual rate of anthropogenic emissions [68]. In China, which is characterized by significant SO_2 outputs from transportation, industry, and other activities [69], assessments of $PCSO_2$ (Per Capita SO_2) emissions [70] have demonstrated that, once applied, policies can effectively reduce SO_2 emissions [71,72]. It is worth noting, however, that the reduction

in SO_2 emissions may lead to an increase in the release of other pollutants resulting from the burning process of alternate fuels such as coal [73].

In a work by Altamira-Colado and collaborators [74], a number of patents based on the implementation of UAS (Uncrewed Aerial Systems, commonly referred to as drones)-compatible SO_2 detectors were reviewed, thus highlighting recent advances in environmental monitoring technology and the possibility of pinpointing sources of SO_2 emissions. Overall, monitoring SO_2 concentrations and their possible sources is therefore important in the assessment of anthropogenic and natural pollution in a given area [75–77]. This study is aimed at the multi-year characterization of SO_2 variability at the World Meteorological Organization—Global Atmosphere Watch (WMO/GAW) regional station of Lamezia Terme (code: LMT) located in the southern Italian region of Calabria. After methane [78] (2016–2022) and ozone [79] (2015–2023), SO_2 is the third compound subject to a detailed multi-year evaluation at the LMT. Using eight years of continuous surface SO_2 measurements (2016–2023), this study also integrates tropospheric column data obtained by satellite to further assess the sources of emission in the area. This paper is divided as follows: Section 2 described the LMT site, its peculiarities in the context of the Mediterranean basin, and the instruments/methodologies used in this evaluation; Section 3 shows the results of the analysis; and Sections 4 and 5 discuss and conclude the findings of this paper, respectively.

2. The Lamezia Terme Station and Surface/Tropospheric SO_2 Databases

2.1. The WMO/GAW Regional Coastal Site of Lamezia Terme

Within the WMO/GAW network, the Lamezia Terme (LMT) regional coastal station located in the municipality of Lamezia Terme in Calabria, Southern Italy, gathers continuous data on a number of meteorological and chemical parameters in the atmosphere. Its coordinates are 38.87 °N, 16.23 °E (Figure 1A), and it has been operated by the National Research Council of Italy—Institute of Atmospheric Sciences and Climate (CNR-ISAC)—since 2015. The observation site is located at an elevation of 6 m above sea level, approximately 600 m from the nearby Tyrrhenian coastline of Calabria. The Catanzaro isthmus where the station is located constitutes the narrowest point in the entire Italian peninsula, as the distance between the Tyrrhenian and Ionian coasts is ≈32 km.

In terms of anthropogenic and natural SO_2 emission hotspots, the area where the LMT station is located is characterized by the presence of the Gioia Tauro port (52 km S–SW from the site) [80] and volcanic activities [81] (Figure 1B). The Mount Etna volcano is located in the nearby region of Sicily (160 km S-SW from the LMT) [82–85]. The Aeolian Arc, which includes the Aeolian Islands and a number of underwater volcanoes [86], many of which have not erupted in historical times, are also close to the LMT. Stromboli (88 km W–SW from LMT) is the nearest active volcano and a well-documented source of SO_2 in the region [87,88]. Vulcano, located in the southernmost part of the Aeolian Islands, has not experienced eruptions in the past few centuries but is subject to SO_2 degassing in the form of fumarole/vents, a phenomenon that also affects Stromboli and Mt. Etna [89–92].

Previous works based on preliminary data [93] and nearly a decade of LMT observations [78,79] have reported the influence of local wind circulation on the surface concentrations of many parameters. In fact, the site is characterized by two distinct wind axes: a western "seaside" wind corridor normally yielding lower concentrations of pollutants, and a northeastern "continental" corridor that is generally linked to the highest peaks observed at the LMT, although notable exceptions have been reported [78,79,94]. The Lamezia Terme International Airport (IATA: SUF; ICAO: LICA), which is located approximately 3 km north from the WMO/GAW station, has an RWY 10/28 (runway 100–280 °N) orientation, and local air traffic is constantly influenced by the same wind circulation patterns reported at the LMT.

Prior to the LMT's continuous atmospheric observations, wind patterns were subject to a number of studies. Locally, wind circulation is dominated by breeze regimes, which also regulate the climate across all seasons, and the Marcellinara Gap in the middle of the Catanzaro isthmus is responsible for channeling wind circulation between the Tyrrhenian and Ionian coasts [95,96]. Although seasonal changes in wind circulation occur, the main corridors at low altitudes are oriented on a NE–ENE/W–WSW axis, while NW large-scale circulation is dominant at the 850 hPa layer [95]. Between November and February, daytime circulation is mainly subject to large-scale forcing, and breezes dominate nocturnal flows; in the other periods of the year (spring, summer, and October), daytime breezes are dominated by both local and large-scale flows [96].

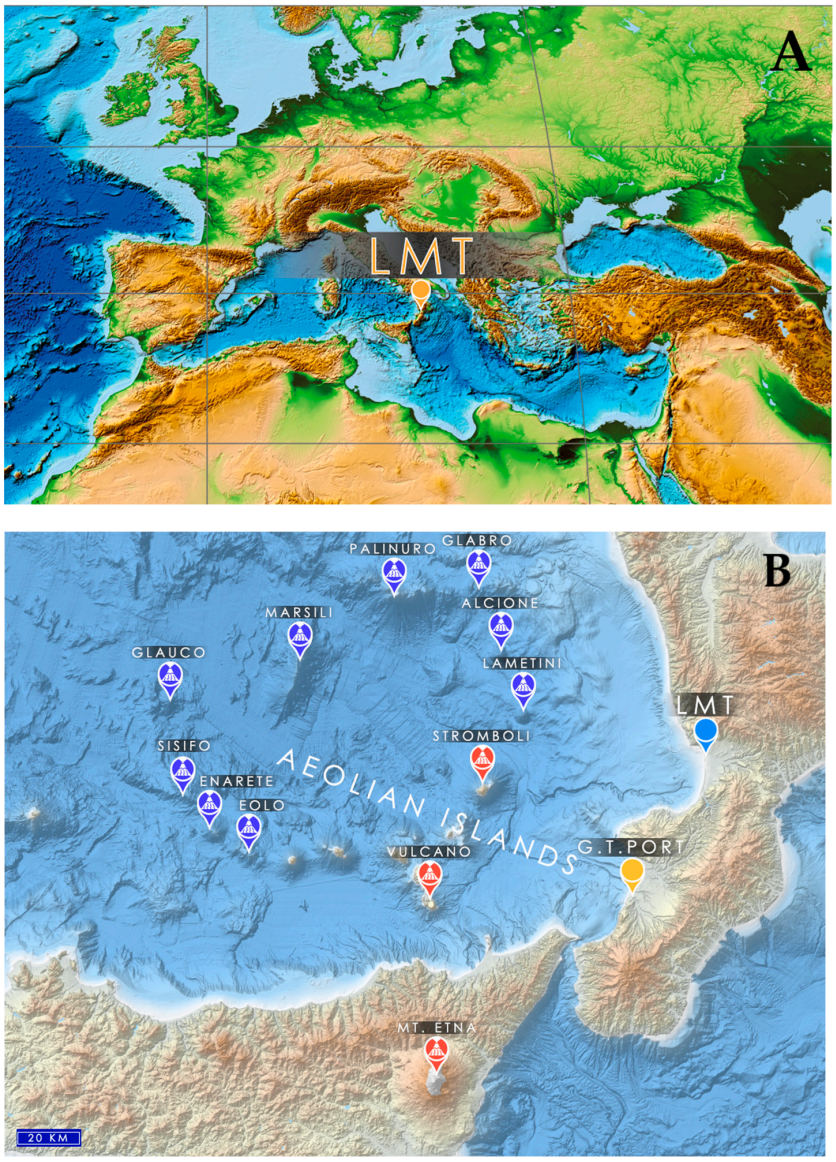

Figure 1. (**A**) Location of Lamezia Terme's observation site (LMT) in the Mediterranean Basin on NOAA's ETOPO1 DEM (Digital Elevation Model) [97,98]. (**B**) EMODnet DEM map [99] showing the location of the LMT in central Calabria and the SO_2 emission hotspots present in the area: the Gioia Tauro Port, Stromboli and Vulcano in the Aeolian Islands, and Mount Etna in Sicily. The main underwater volcanoes in the arc are marked with dark blue labels. "Lametini" refers to the two twin underwater volcanoes (LamN and LamS) named after the municipality of Lamezia Terme. Local maps showing sources of pollution in the Lamezia Terme municipality area with greater detail are available from D'Amico et al. (2024a) [78], (2024b) [100], (2024c) [94].

Following the introduction of surface measurements of greenhouse gases (GHGs) and other parameters at the LMT in 2015, additional campaigns targeted the enhanced characterization of local wind circulation at low altitudes. Using a Zephir lidar 300, several wind profiles have been observed at the site at various altitude thresholds, from 10 to 300 m above the ground level [101]. Additionally, based on the results of a short 2009 summertime campaign performed via the implementation of multiple techniques and instruments, two evaluations of PBL (planetary boundary layer) variability at the site were conducted [102,103]. These studies, however, lacked information on additional parameters, which were, however, covered in a longer 2024 campaign on integrated PBL/GHG/aerosol variability that demonstrated the influence of PBLH (PBL height) and wind regime categories on LMT observations [104].

Prior to this research study and the assessment of possible volcanic activity influence on the LMT, multiple local sources of pollution have been mentioned in the past as responsible for some of the peaks observed at the site. Landfills, agricultural and livestock farming, the A2 highway, the SUF/LICA airport, and urban traffic in the town center have been reported in various studies as possible sources of certain peaks [78,93,100]. Specifically, many of the hypotheses on these sources were confirmed in an analysis of the first 2020 COVID-19 lockdown period, during which the restrictions introduced by the Italian government were strict and allowed researchers to better assess a number of pollution sources in a period of exceptionally low anthropic activities [94]. Furthermore, in considering the location of the site in the context of the Mediterranean basin, summer open-fire emissions [105,106] and Saharan dust events [107] have also characterized LMT observations.

2.2. Measurements of Surface Sulfur Dioxide and Meteorological Parameters

SO_2 concentrations at the LMT observation site have been gathered with a Thermo Scientific 32i (Franklin, MA, USA). The 43i model operates under the principle by which SO_2 molecules in ambient air absorb ultraviolet (UV) light, consequently becoming excited, at a specific wavelength and emit additional UV light at a given wavelength during their decay to a lower energy state. Specifically, sample air in the 43i model flows through a hydrocarbon (HC) "kicker" that removes HC from gathered ambient air by forcing these compounds to permeate through the kicker tube wall, while SO_2 molecules are unaffected by the filter. The standard flow rate is 0.5 L per minute. Ambient air is then channeled toward a fluorescence chamber where UV light pulses excite SO_2 molecules. A condensing lens, following these pulses, focuses UV light on the mirror assembly, which contains four selective mirrors that reflect only the wavelength capable of exciting SO_2 molecules. As described above, following the absorption of UV light, SO_2 molecules decay and emit UV at an intensity that is proportional to SO_2 concentration within the chamber. Thanks to a bandpass filter, only the wavelengths emitted by excited SO_2 in sampled air can reach the PMT (photomultiplier tube), which detects UV light emissions attributable only to these decaying molecules. A photodetector located at the back of the fluorescence chamber is configured to monitor UV light pulses and is connected to a compensation circuit that counterbalances fluctuations in UV light. The sampled ambient air moves from the chamber to a flow sensor, followed by a capillary and the exhaust bulkhead. The instrument provides, at a rate of ten measurements per minute (one every six seconds), observed SO_2 concentrations and stores them in a record for further data analysis. The detection limit is <0.5 ppb of SO_2. In this research study, data were aggregated on an hourly, daily, monthly, seasonal, or yearly basis depending on each evaluation.

A Vaisala WXT520 (Vantaa, Finland) instrument was used to gather data on key meteorological parameters (wind speed, wind direction, relative humidity, and air temperature) at 10 m above sea level, with no obstacles nearby at the same elevation. The WXT520

measures temperature in Celsius degrees with a precision of 0.3 °C via an RC oscillator and two reference capacitors. Wind data were obtained using ultrasonic transducers placed on a horizontal plane. Wind speed was measured with a precision of 0.3 m per second, while wind direction had a precision of 3 degrees. Additional details on WXT520 measurements at the LMT are available from D'Amico et al. (2024c) [94]. Data aggregation algorithms were applied to meteorological data depending on the evaluation type (hourly, daily, etc.).

As described in Section 2.1, the LMT observation site is characterized by a daily cycle that results in a clear differentiation between western–seaside and northeastern–continental winds, which in turn result in differences in a number of parameters [78]. Figure 2A shows a wind rose of hourly data gathered between 2016 and 2023, and the presence of two distinct wind corridors is noticeable.

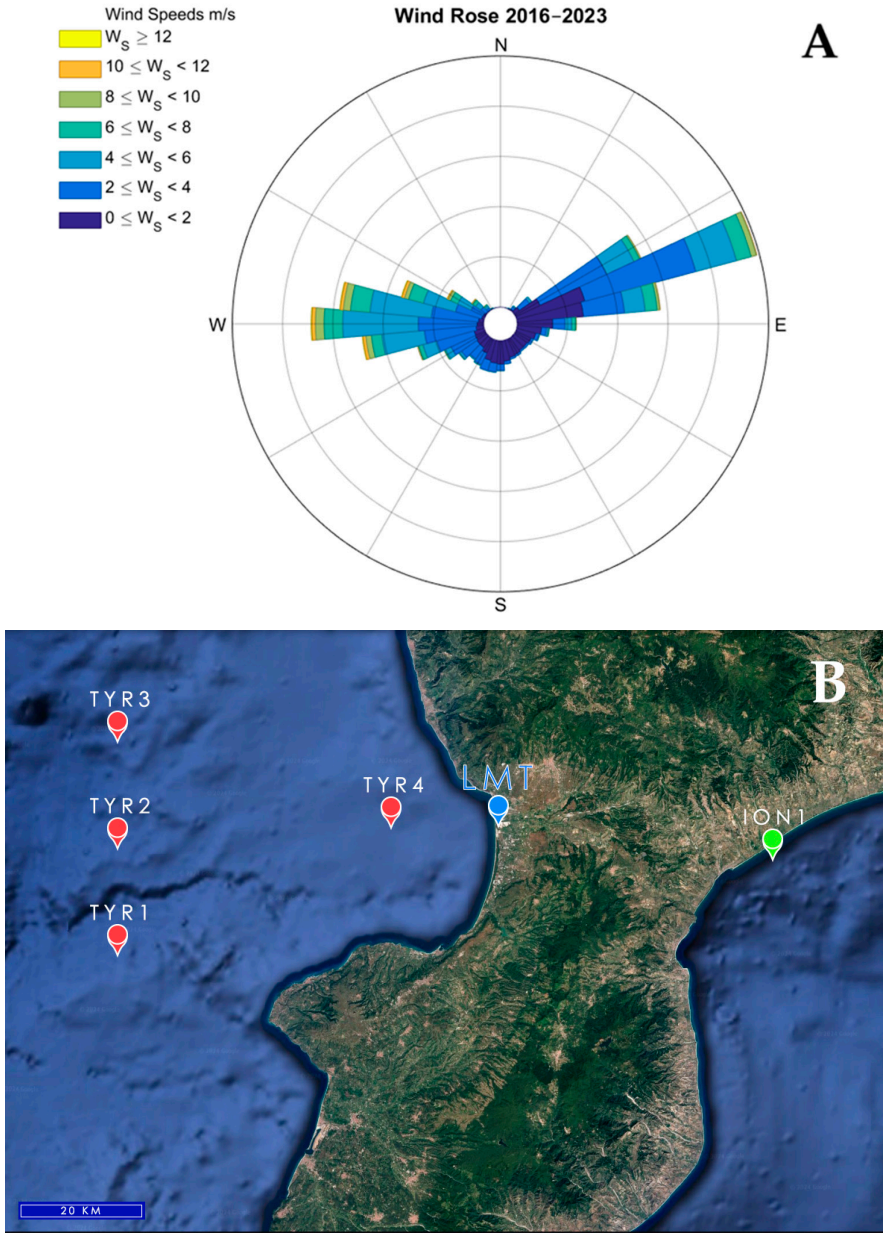

Figure 2. (**A**) Wind rose of frequency counts and wind speed thresholds, based on hourly data gathered at the LMT with Vaisala WXT520 equipment between 2016 and 2023. The bars have an angle of 8 degrees each. (**B**) Locations of the TYR1–4 (Tyrrhenian) and ION1 (Ionian) points used for the comparison of surface mole fractions of SO_2 with satellite tropospheric column data.

The western wind corridor, which has virtually no obstacles in that direction for hundreds of kilometers, has been used as a baseline to define an offshore cone aimed at satellite data evaluation. The points TYR1–3 located 60 km west from the coast, point TYR4 located 3 km west from the observatory, and point ION1 in the Ionian coast of the Catanzaro isthmus are shown in Figure 2B. These points are considered representative of the airmasses passing at the LMT observatory from both wind corridors. In particular, due to local wind circulation in the isthmus being channeled through the Marcellinara Gap, point ION1 is considered representative of eastern air masses prior to the influence of anthropogenic emissions in continental Italy.

Following other studies based on multi-year evaluations on LMT data [78,79], the four seasons were divided as follows: summer (JJA—June, July, August); fall (SON—September, October, November); winter (JFD—January, February, December); spring (MAM—March, April, May).

Additional details on the data gathered at the LMT during the observation period 2016–2023 are available in Table 1, which reports the coverage rate of Thermo Scientific 43i ("SO_2") and Vaisala WXT520 ("Meteo") instruments and their percentages of the total number of hours in each year. The "Combined" dataset, used for data evaluations accounting for both SO_2 concentrations and wind speed/direction, refers to instances of both instruments fully operating at the same time, therefore resulting in overall lower coverage rates. Due to maintenance, the SO_2 dataset was affected by low rates in 2019, 2022, and 2023; however, the high coverage rate of the Meteo dataset throughout the entire study period ensured a minimum additional loss of coverage in the Combined set. Furthermore, wind direction filters were applied to differentiate the western–seaside corridor (240–300 °N) at the observation site of the LMT from the northeastern–continental corridor (0–90 °N).

Table 1. Coverage rates, shown as percentages compared to the actual number of hours, of the three datasets used in this study. Both 2016 and 2020 are leap years, with 24 extra hours each.

Year	Hours	SO_2 (%)	Meteo (%)	Combined (%)
2016	8784	95.53%	96.34%	93.54%
2017	8760	97%	93.8%	92.42%
2018	8760	80.59%	77.05%	58.21%
2019	8760	40.23%	98.59%	40.21%
2020	8784	93.47%	99.98%	93.46%
2021	8760	70.78%	99.74%	70.77%
2022	8760	66.65%	89.85%	65.34%
2023	8760	51.31%	96.3%	49.92%
Total	70,128 [1]	74.44% [2]	93.95% [2]	70.48% [2]

[1] Sum of all hours. [2] Average rate.

Data aggregation algorithms were used in R 4.4.0 using the ggplot2, ggpubr, tidyverse, and dplyr libraries and their respective packages. The aggregations were based on the data analyses performed on multi-year methane [78] and ozone [79] concentrations at the same observation site. In this research, evaluations showing SO_2 data alone were based on the SO_2 dataset from Table 1, while those combining SO_2 concentrations with meteorological data were based on the Combined dataset. All hours are in UTC.

2.3. Tropospheric Column Measurements of SO_2

On 13 October 2017, the TROPOspheric Monitoring Instrument (TROPOMI) installed onboard the Sentinel-5P satellite, under the ESA's Copernicus program, was launched [108]. The satellite and instrument carried out detailed analyses on the SO_2, CH_4 (methane), CO (carbon monoxide), O_3 (ozone), NO_2 (nitrogen dioxide), and HCHO (formaldehyde)

concentrations in the atmosphere. The TROPOMI is a remote sensing instrument of the "passive" type, equipped with a hyperspectral nadir sensor of several UV-Vis-NIR spectrometers. Specifically, the advanced instrument relies on four spectrometers set at two bands: SWIR (2305–2385 nanometers, nm); UV and Vis (270–495 nm); and NIR (675–775 nm). The spatial resolution is in the 5–15 km range, with an option for 50 km at wavelengths lower than 300 nanometers [109].

The instrument images a swath for about one second, yielding a spatial resolution at the center of the swath of 7×7 km^2. The results of the TROPOMI scans were processed with an algorithm providing accurate vertical column densities, or VCDs, in molecules per square centimeter (molecules/cm^2) of the SO_2, CO, and NO_2 [110]. Study areas were processed with one full scan, with an option for two partial scans; available data were used in this research using level 2 TROPOMI products from 1 January 2020 to 31 December 2023, in accordance with the recommendations and technical documents provided with these products [111]. Column density data in molecules per square meter (molecules/m^2) were converted into molecules per square centimeter (molecules/cm^2) using the multiplication factor of 6.02214×10^{19} recommended by the ESA [112].

Downloaded products were processed with an algorithm programmed in MATLAB-R2016a, based on a number of steps that have also been used in a summer campaign on formaldehyde tropospheric column data at the LMT [113]. Specifically, the steps were the following: TROPOMI products were downloaded in netCDF format and parsed through; coordinates and time were extracted from the products and converted; data on the tropospheric gas density were extracted from the matrix and stored in a georeferenced array; the entire dataset was filtered; and all data with a Quality Assurance Value (Q_a) lower than 0.5 were excluded. Q_a, and its related qa_value flag in the dataset, is a data quality value ranging from 0 to 1 that accounts for several factors. As per the recommendations, only data with Q_a >0.5 were used for further evaluation in this study, representative of the following conditions: Solar Zenith Angle (SZA) $\leq 70°$; air mass factor > 0.1; cloud radiance fraction at 340 nm <0.5; surface albedo ≤ 0.2; no error flag; no snow/ice warning. In this work, tropospheric column data from the LMT's coordinates, as well as the coordinates of the TYR1–4 and ION1 points shown in Figure 2B, were selected, and their coverage rate is reported in Table 2. Additional details on the algorithm and its evaluations are available from Barrese et al. (2024) [113].

Table 2. Coverage rate, shown as a percentage of the total number of days in a given year, of TROPOMI satellite data on SO_2 concentrations; 2020 was a leap year, with one extra day.

Year	Days	Sat. SO_2 (%)
2020	366	38.25%
2021	365	34.52%
2022	365	42.73%
2023	365	38.08%
Total	1461 [1]	38.39% [2]

[1] Sum of days. [2] Average rate.

In order to show the large-scale influence of natural sources such as volcanoes in the area, Level 3 (L3) products were used to generate yearly maps of SO_2 [114]. Specifically, maps referring to the period 2020–2023 were generated based on the COvariance-Based Retrieval Algorithm (COBRA) developed to compensate for a number of artifacts in Differential Optical Absorption Spectroscopy (DOAS) of SO_2 via the retrieval of one specific parameter, which was the SO_2 Slant Column Density (SCD) [115,116].

3. Results

3.1. Daily Cycles of Sulfur Dioxide at LMT

As described in Section 2, the LMT observation site is affected by local wind circulation patterns, which results in peculiar daily cycle for gases and aerosols at the site. The characterization of daily cycles based on multi-year data on methane [78] and ozone [79] showed two distinct behaviors. Figure 3 shows the results of SO_2 daily cycle analysis at the LMT.

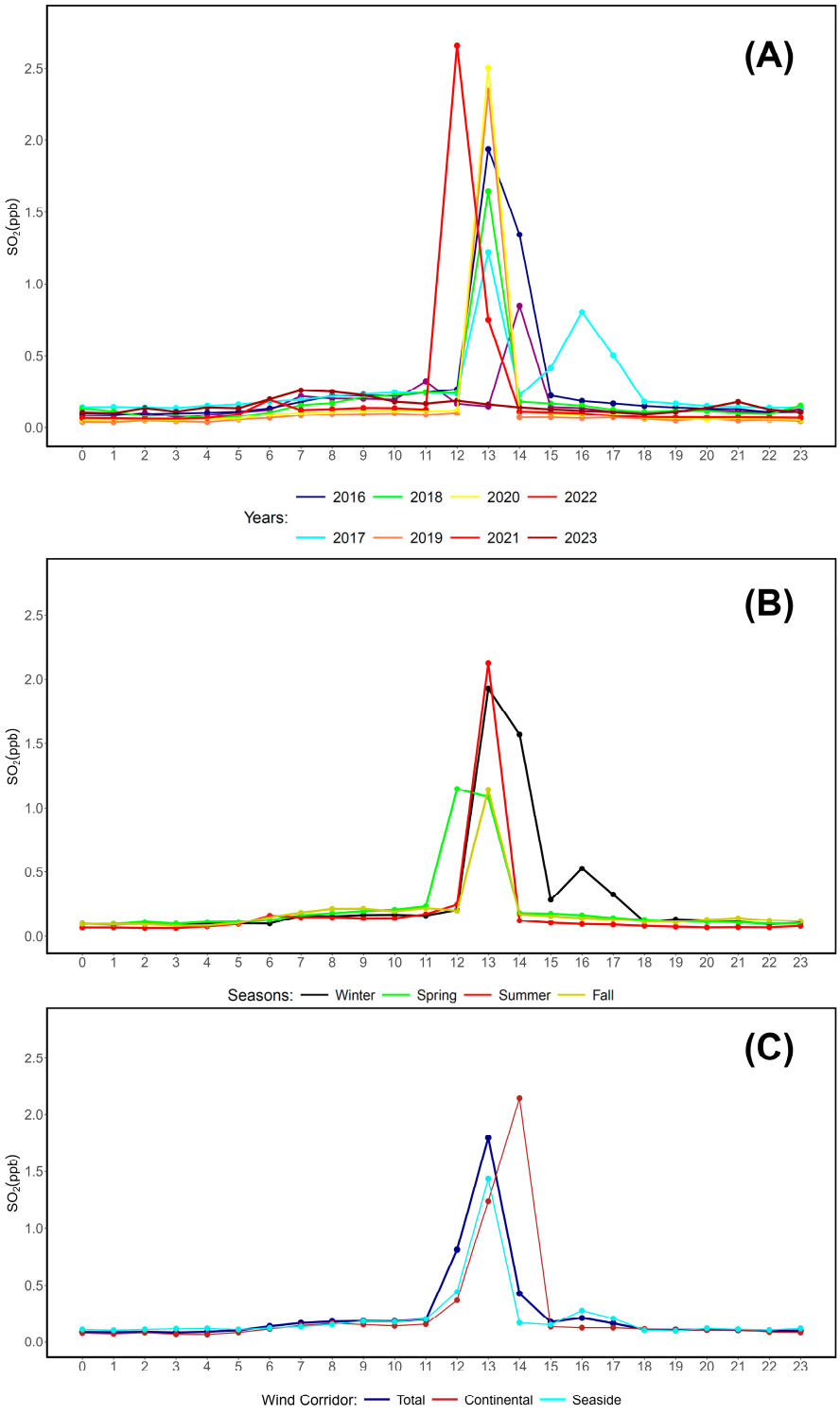

Figure 3. (**A**) Daily cycle of SO_2 at the LMT based on the year of evaluation. (**B**) Seasonal daily cycle. (**C**) Daily cycle differentiated by wind corridor, using both SO_2 and meteorological data.

Overall, the daily cycle of SO_2 is unlike the cycles observed for methane and ozone, although ozone shows a similar behavior in diurnal peaks [79]. In this case, the peaks are narrowed down in a specific time window (11:00–15:00 UTC). The behavior of SO_2 with respect to the daily cycle at the LMT demonstrates the importance of compound-specific evaluations using multi-year datasets, as the variability of each observed compound at the site possessed certain distinctive properties.

3.2. Bivariate Analysis with Wind Direction and Speed

In integrating the data shown in the wind rose based on 2016–2023 hourly averages (Figure 2), which is thus representative of eight years of local wind circulation at the LMT, a total of four seasonal wind rose scatter plots of SO_2 are shown in Figure 4. These plots, which integrate the daily cycle evaluations seen in 3.1, show SO_2 concentrations from the western–seaside wind corridor at wind speeds higher than their northeastern–continental counterparts. Supplementary Materials S1A–H cover seasonal patterns in each year between 2016 and 2023.

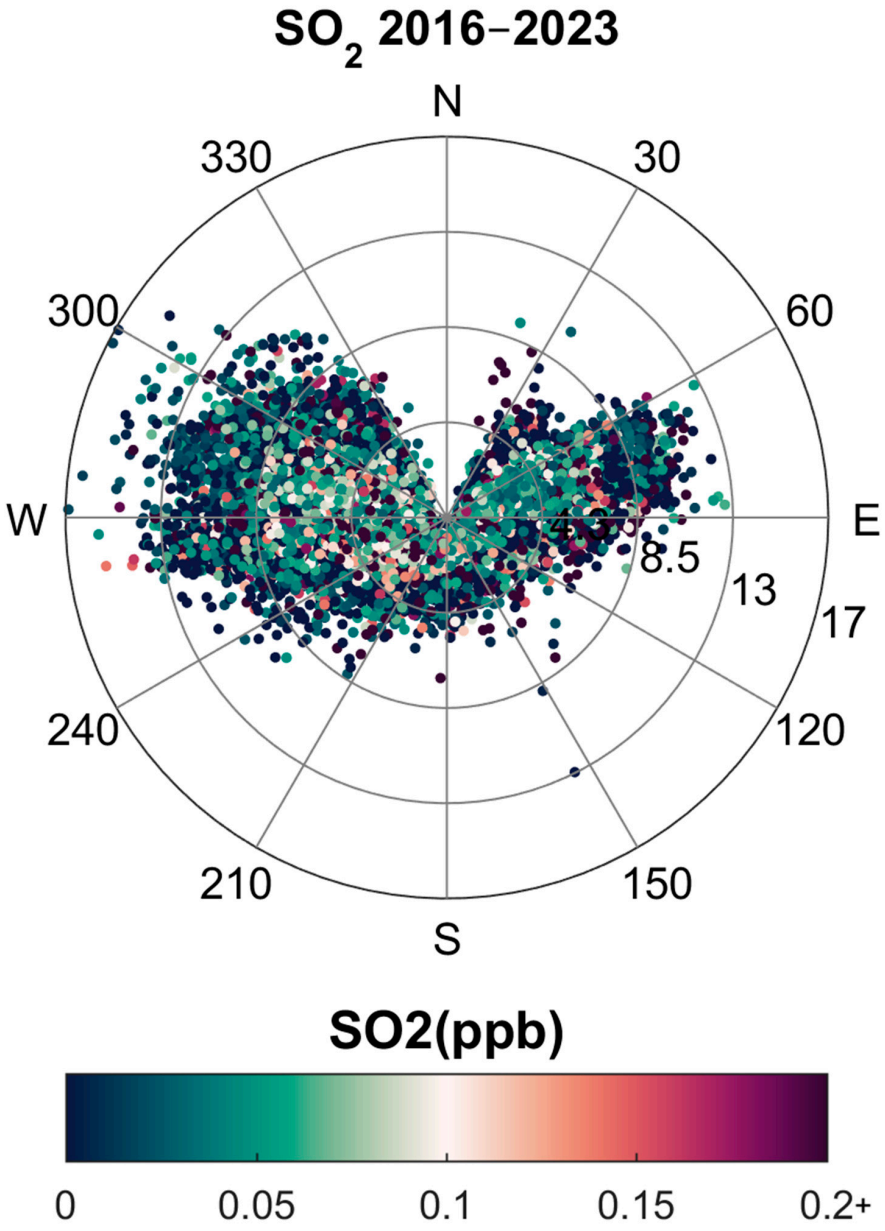

Figure 4. *Cont.*

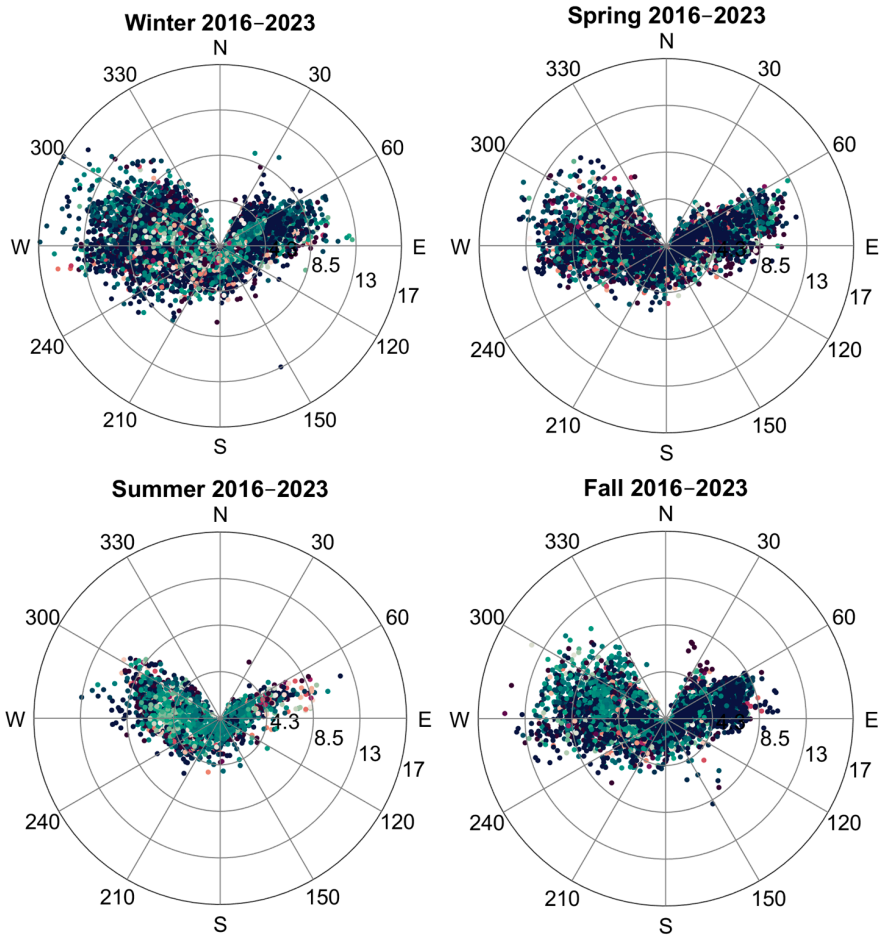

Figure 4. Total (**top**) and seasonal (**bottom**) wind rose scatter plots of observed SO_2 mole fractions at Lamezia Terme (LMT), with respect to wind speeds and directions. In order to optimize visualization, the color scale bar's maximum value of 0.2+ ppb is defined based on the average reported value of 0.217 ppb (see Section 3.5).

D'Amico et al. (2024a) [78] showed that methane concentrations at the LMT from the northeastern–continental sector follow a hyperbola branch pattern (HBP), with low wind speeds correlated with high concentrations and, vice versa, high wind speeds yielding very low mole fractions. The same pattern was not observed from the western–seaside air corridor. An identical analysis was performed by D'Amico et al. (2024d) [79] on surface ozone and did not show any evidence of a similar pattern. Eight years of continuous surface SO_2 records at the LMT were tested, as shown in Figure 5, with respect to wind speeds and wind corridor. Figure 5A,B refer to the W and NE sectors, respectively, while Figure 5C considers all data, including those falling outside the W and NE filters. Supplementary Materials S2A1–H3 cover the entire 2016–2023 period.

As already reported for the daily cycle, the observed behavior of SO_2 at the LMT observation site is different from that of methane and surface ozone. Specifically, the variability of SO_2 with respect to wind speed at the site from all sectors is not as well defined as that observed for methane [78].

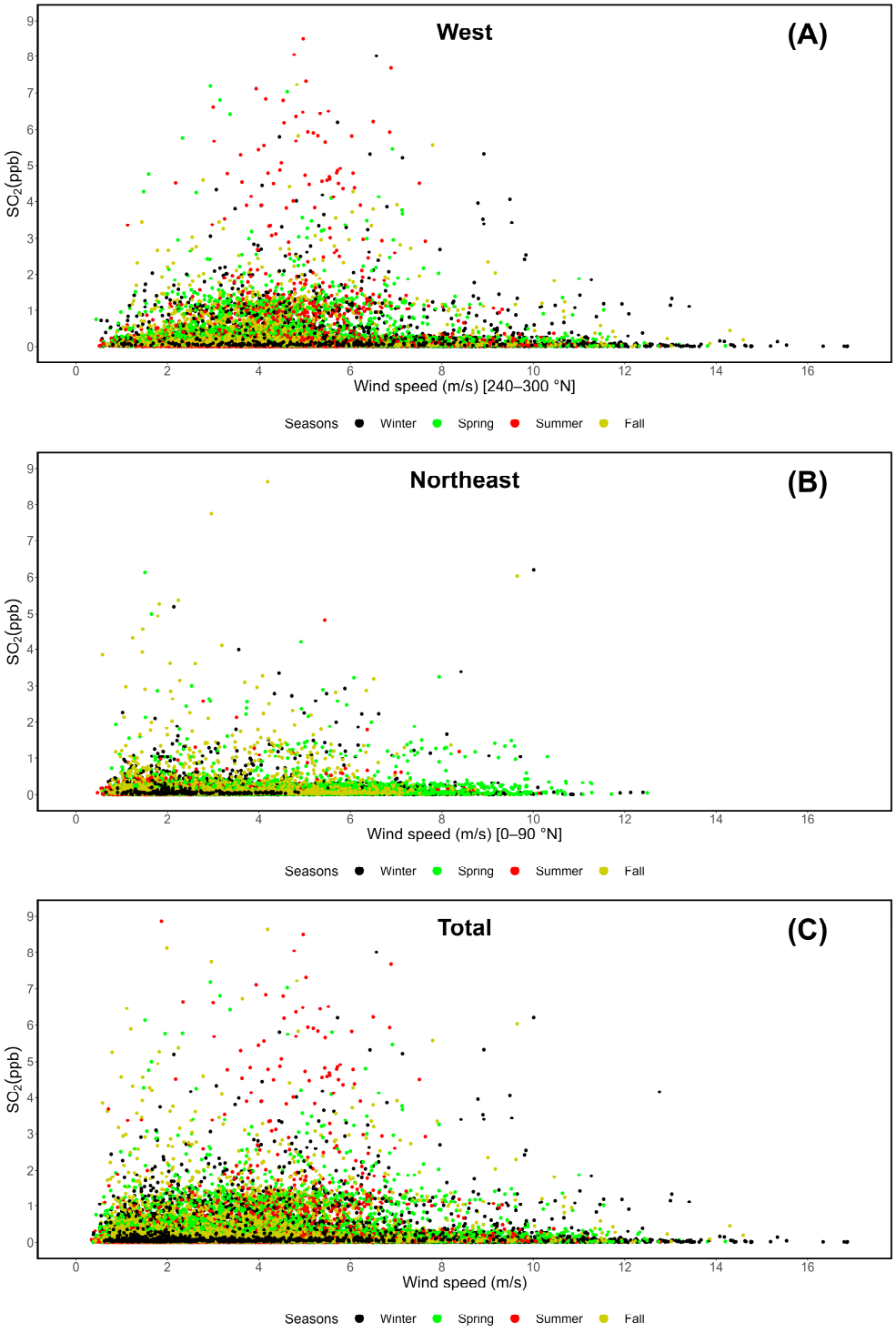

Figure 5. SO_2 concentrations and wind speed variability on a wind corridor basis. (**A**) Western "seaside" (240–300 °N); (**B**) northeastern "continental" (0–90 °N); (**C**) total data, including those falling outside the two wind direction filters.

3.3. Evaluation of Weekly Cycles of SO_2 at LMT

Multi-year evaluations of compounds at the LMT have also been conducted on the weekly cycles as possible indicators of natural vs. anthropogenic sources [78,79,100]. In the case of SO_2, considering the implementation of satellite data that were not used in similar research studies on the LMT, weekly cycles were assessed and are shown in Figure 6. Supplementary Materials S3A1–H3 cover surface data at the LMT from each year within the entire 2016–2023 observation period.

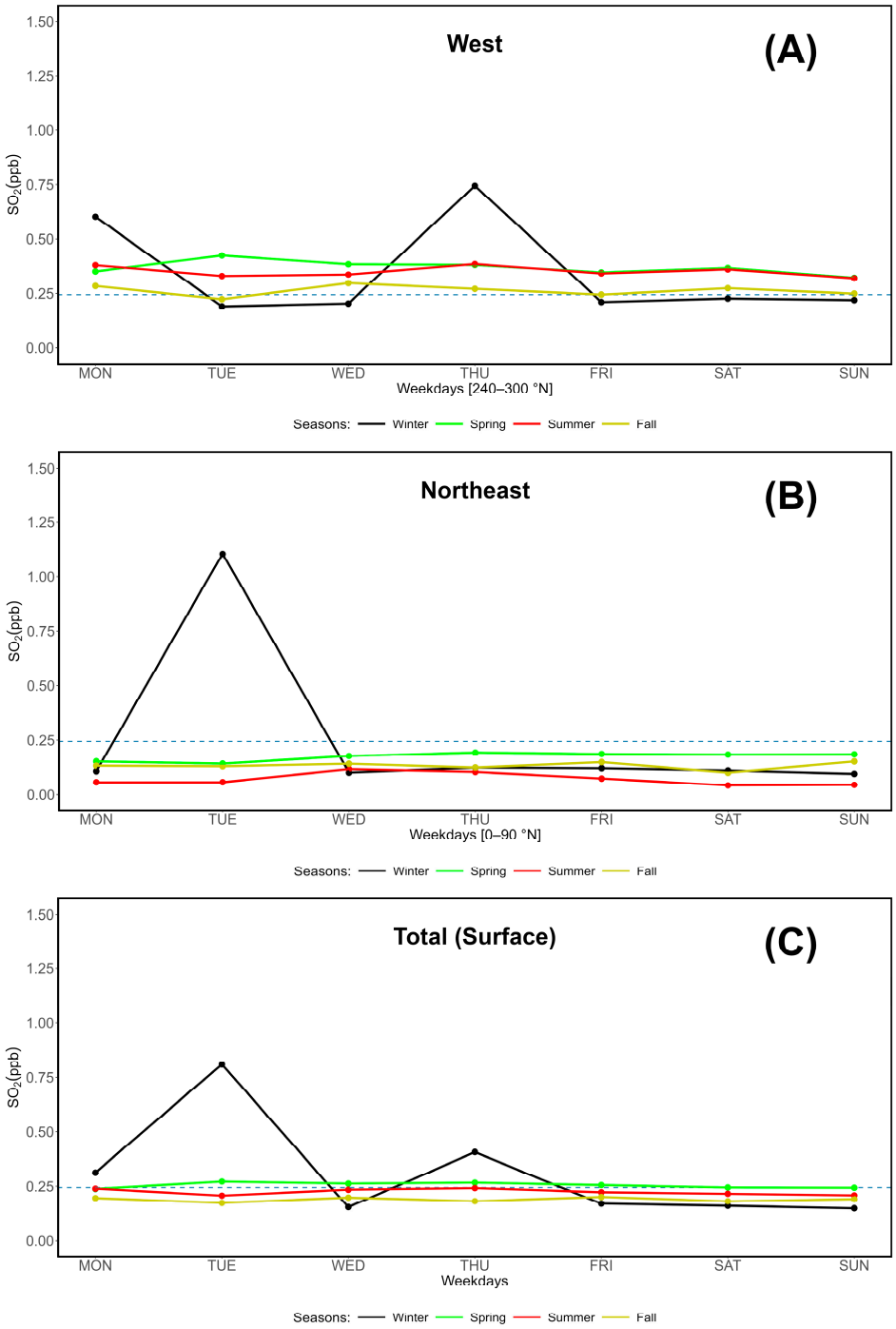

Figure 6. *Cont.*

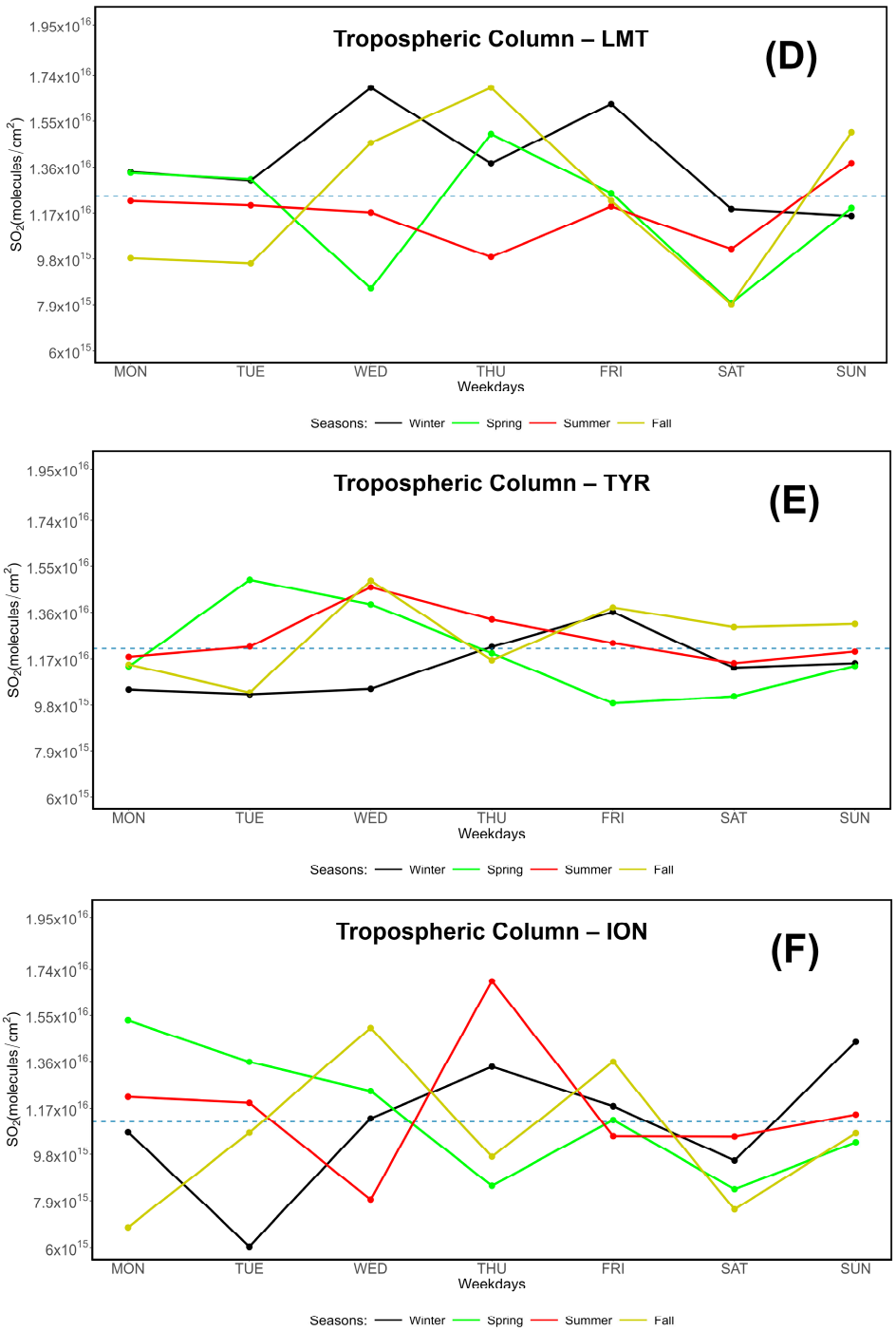

Figure 6. Weekly cycle evaluation of surface and tropospheric column SO_2 at the LMT and the TYR-ION coordinates, with the dotted horizontal lines showing the averages. (**A**) Surface, western "seaside" corridor (240–300 °N); (**B**) surface, northeastern "continental" corridor (0–90 °N); (**C**) surface, total data; (**D**) column, at LMT; (**E**) column, based on averages of TYR points; (**F**) column, ION1.

The analysis of surface data does not shown specific weekly patterns, with the exception of a number of spikes falling outside weekends. Tropospheric column data are more heterogeneous and show various fluctuations mostly affecting the LMT and ION data. At the LMT, weekly trends and their respective seasonal changes have been observed frequently, especially in the case of greenhouse gases and aerosols; the absence of a well-defined weekly variability pattern is linked to natural sources, which tend to be spread equally over the course of a standard week [100].

3.4. Variability During the Observation Period

After specific evaluations aimed at daily, weekly, and seasonal trends, in conjunction with the cross-analysis with wind data, the multi-year variability of SO_2 at the LMT was assessed, and the results of the surface data are shown in Figure 7. The plots are based on past research studies at the site, which demonstrate the presence of wind sector-dependent concentrations of gases and aerosols, which in turn indicates the presence of multiple sources of pollution [104].

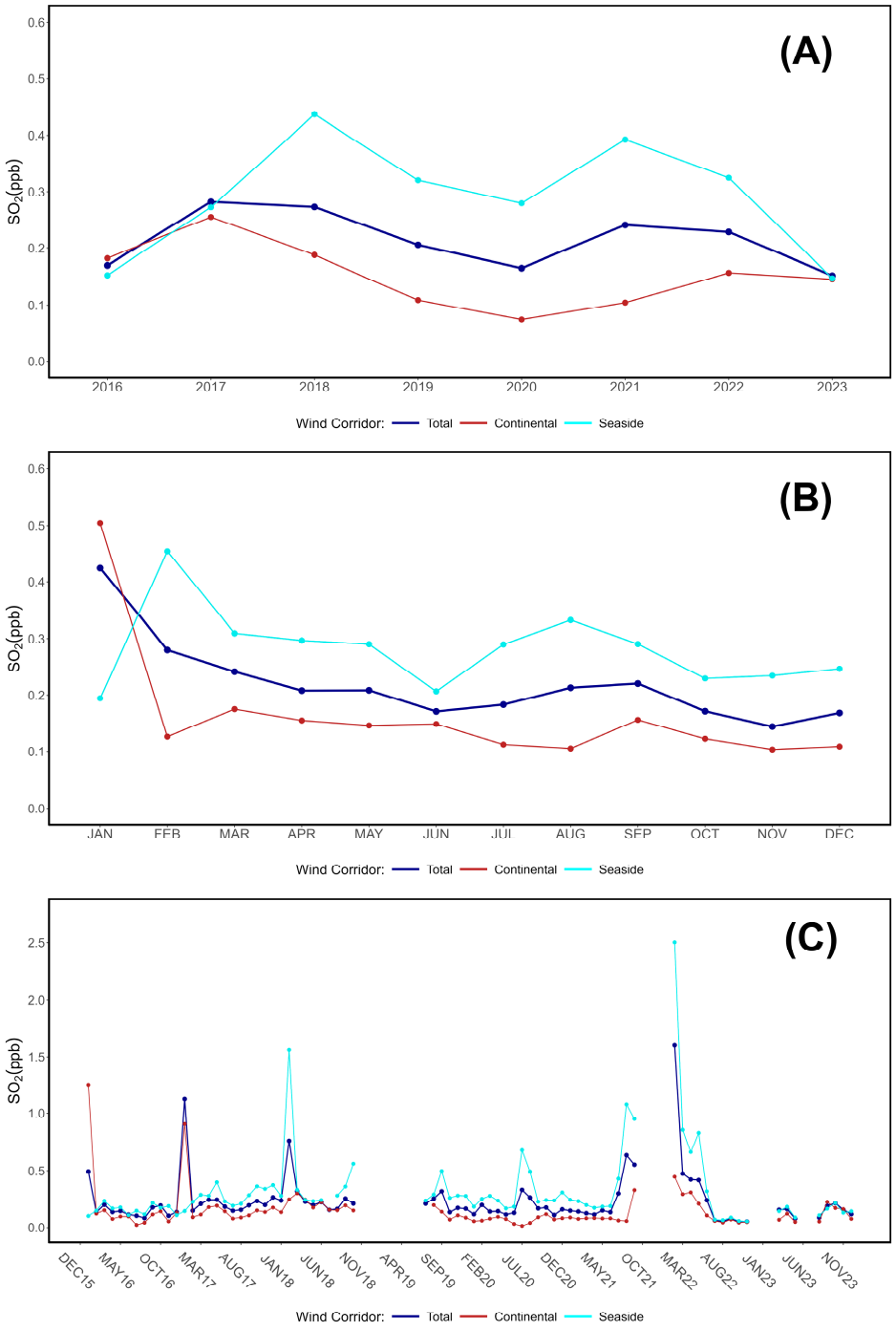

Figure 7. Multi-year variability of surface SO_2 concentrations at the Lamezia Terme WMO/GAW station differentiated by wind corridor. (**A**) Yearly averages between 2016 and 2023. (**B**) Seasonal cycle. (**C**) Monthly averages.

Tropospheric column densities gathered between 2020 and 2023 at the designated LMT, TYR, and ION locations were also analyzed to monitor multi-year variability, and the results are shown in Figure 8. This methodology was not applied to studies on the multi-year variability of other compounds previously assessed at the LMT. Specifically, in Figure 8A, the monthly variability of the total SO_2 column measured by satellite is reported.

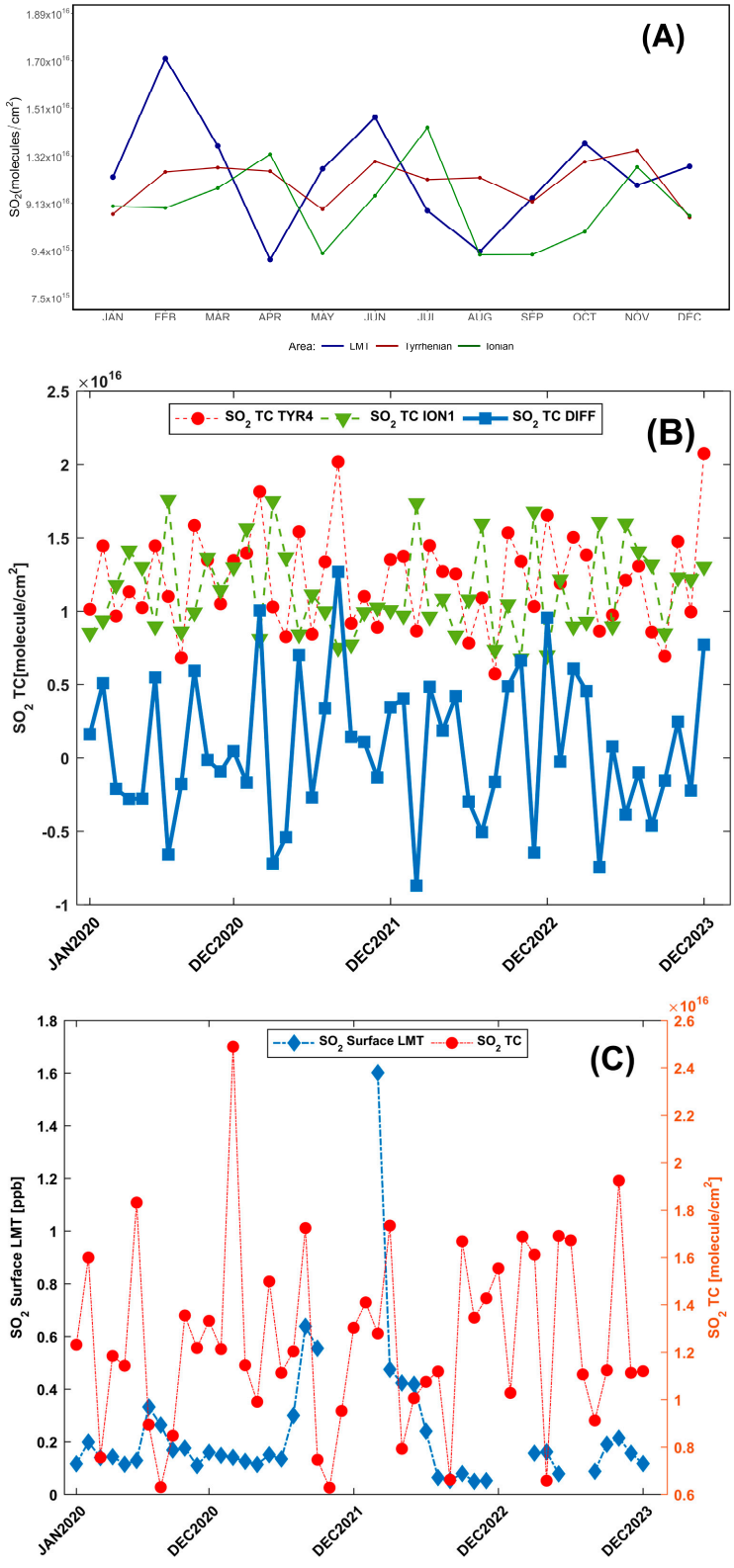

Figure 8. *Cont.*

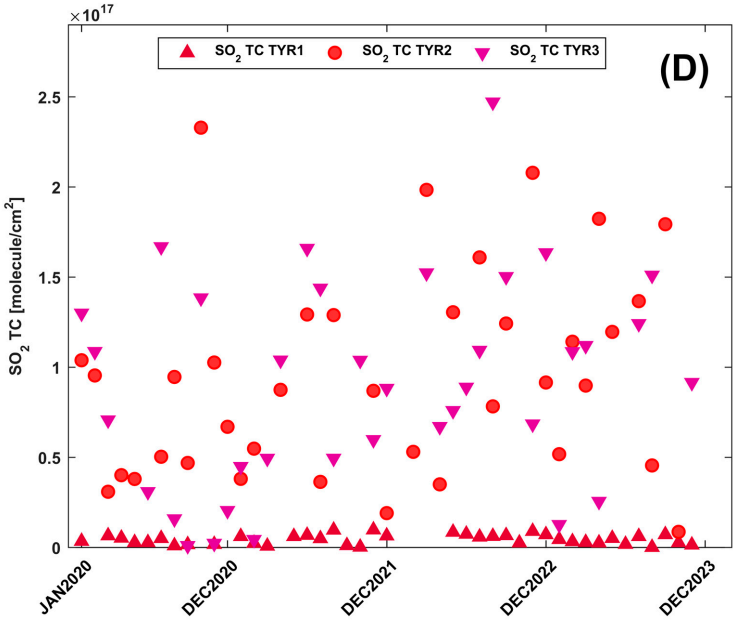

Figure 8. Multi-year variability of tropospheric column data. (**A**) Monthly variability. (**B**) $TCSO_2$ monthly means measured at TYR4 and ION1, and their respective differences. (**C**) Direct comparison between LMT surface and column SO_2 concentrations. (**D**) Variability of the column data from the three TYR points in the Tyrrhenian Sea, located close to the Aeolian Arc.

To highlight the differences between the two Calabrian coasts and broadly identify sources of SO_2 emissions, in Figure 8B, the monthly means of $TCSO_2$ (Total Column SO_2) at points TYR4 and ION1 are reported. A comparison between the in situ (surface) SO_2 concentration data and satellite tropospheric column data is shown in Figure 8C. In Figure 8D, points TYR1–3 are analyzed, which are further away from the Tyrrhenian coast (Figure 2), in order to highlight possible SO_2 outputs from maritime shipping and volcanic sources. These points are representative of the western–seaside sector of the LMT, while ION1 is deemed representative of easterly air masses prior to their contact with the continent, which results in increased anthropogenic influence. The plots indicate that TYR1, whose distance to the Stromboli volcano is similar to that of TYR2, is less subject to the transport of air masses enriched in SO_2.

3.5. Statistical Evaluations

The findings of this study were subjected to a statistical evaluation performed using Jamovi v. 2.3. Key surface SO_2 and meteorological data gathered during the entire observation period (2016–2023) were evaluated to determine the mean, median, variance, standard deviation (SD), and quantiles. Pearson's Correlation Coefficient (PCC) and Spearman's Rank Correlation Coefficient (SR) were also calculated to test a number of correlations between the chemical and meteorological data [117–119].

Regarding the SR, particularly for a sample of size n, the observed variables x and y are converted into ranks (Rx and Ry, respectively); the SR itself ρ is then calculated as described in Equation (1):

$$\rho = (\mathrm{cov}(R_x,R_y))/(\sigma R_x\ \sigma R_y) \quad (1)$$

where "cov" refers to the covariance of both rank variables, and the two values σRx-σRy are the respective standard deviations. The SR ranges between −1 and 1, and its statistical interpretation is similar to that of PCC. The results of the primary statistical evaluation are shown in Table 3. These refer specifically to surface measurements at the LMT site.

Table 3. Main statistical analysis of hourly surface SO_2 and meteorological parameters (RH, relative humidity; T, air temperature; WS, wind speed) in the study period 2016–2023; 1st Q. and 3rd Q. refer to the first and third quartiles, respectively.

	N	Missing	Mean	Median	SD	1st Q.	3rd Q.
RH (%)	66,033	6660	67.442	68.950	11.68	60.890	76.250
T (°C)	66,033	6660	17.784	17.210	6.22	13.380	22.660
SO_2 (ppb)	52,267	20,426	0.217	0.056	2.83	0.028	0.142
WS (m/s)	65,895	6798	3.413	2.97	2.07	1.79	4.55

The results of PCC and SR evaluations on surface measurements are shown in Table 4, which also reports the *p*-values of each pair. The null hypothesis is that the reported variables do not have a direct correlation; statistically relevant *p*-values (<0.05) show the presence of a correlation between the variables in the pair. Most of the computed *p*-values are lower than 0.001; however, a peak of 0.89 is observed for SO_2 and air temperature.

Table 4. Correlation matrix combining surface SO_2 data and key meteorological parameters measured during the observation period 2016–2023. The evaluation shows Pearson's Correlation Coefficient (PCC) and Spearman's Rank Correlation Coefficient (SR).

		WS (m/s)	T (°C)	RH (%)
T (°C)	PCC	0.062 ***	–	–
	p-value	<0.001	–	–
	SR	0.091 ***	–	–
	N	65,893	–	–
RH (%)	PCC	−0.282 ***	−0.175 ***	–
	p-value	<0.001	<0.001	–
	SR	−0.371 ***	−0.200 ***	–
	N	65,893	66,031	–
SO_2 (ppb)	PCC	0.020 ***	0.001	−0.038 ***
	p-value	<0.001	0.89	<0.001
	SR	0.056 ***	0.096 ***	−0.260 ***
	N	49,485	49,623	49,623

*** $p < 0.001$.

A similar approach was applied to satellite data, which are limited in coverage to the 2020–2023 period. The primary statistical information of the satellite (Tropospheric Vertical Column, TVC) data of SO_2 and surface data limited to 2020–2023 are shown in Table 5.

Table 5. Main statistical evaluations of surface and tropospheric column SO_2 between 2020 and 2023.

SO_2 Type	Mean	Median	SD	1st Q.	3rd Q.
Surface (ppb)	0.19	0.11	0.23	0.082	0.19
Trop. Column (molecules/cm^2)	1.24×10^{16}	9×10^{15}	1.13×10^{16}	5.15×10^{15}	1.63×10^{16}

The correlation between the surface and tropospheric column data of SO_2 was tested, and the results are shown in Table 6.

Table 6. Correlation matrix of surface and tropospheric column SO_2, including Pearson's Correlation Coefficient (PCC) and Spearman's Rank Correlation Coefficient (SR).

		Trop. Column (Molecules/cm^2)
Surface (ppb)	PCC	0.042
	p-value	0.324
	SR	0.085 *

* $p < 0.05$.

3.6. Multi-Year COBRA Maps of Volcanic SO_2

In addition to punctual data analysis, maps computed using COBRA [115,116] are shown in Figure 9, referring to each year between 2020 and 2023. These maps rely on Level 3 (L3) products by Sentinel-5P to highlight dominant SO_2 tropospheric circulation in the area; volcanic activity, mostly attributable to Mount Etna, yields the most relevant results.

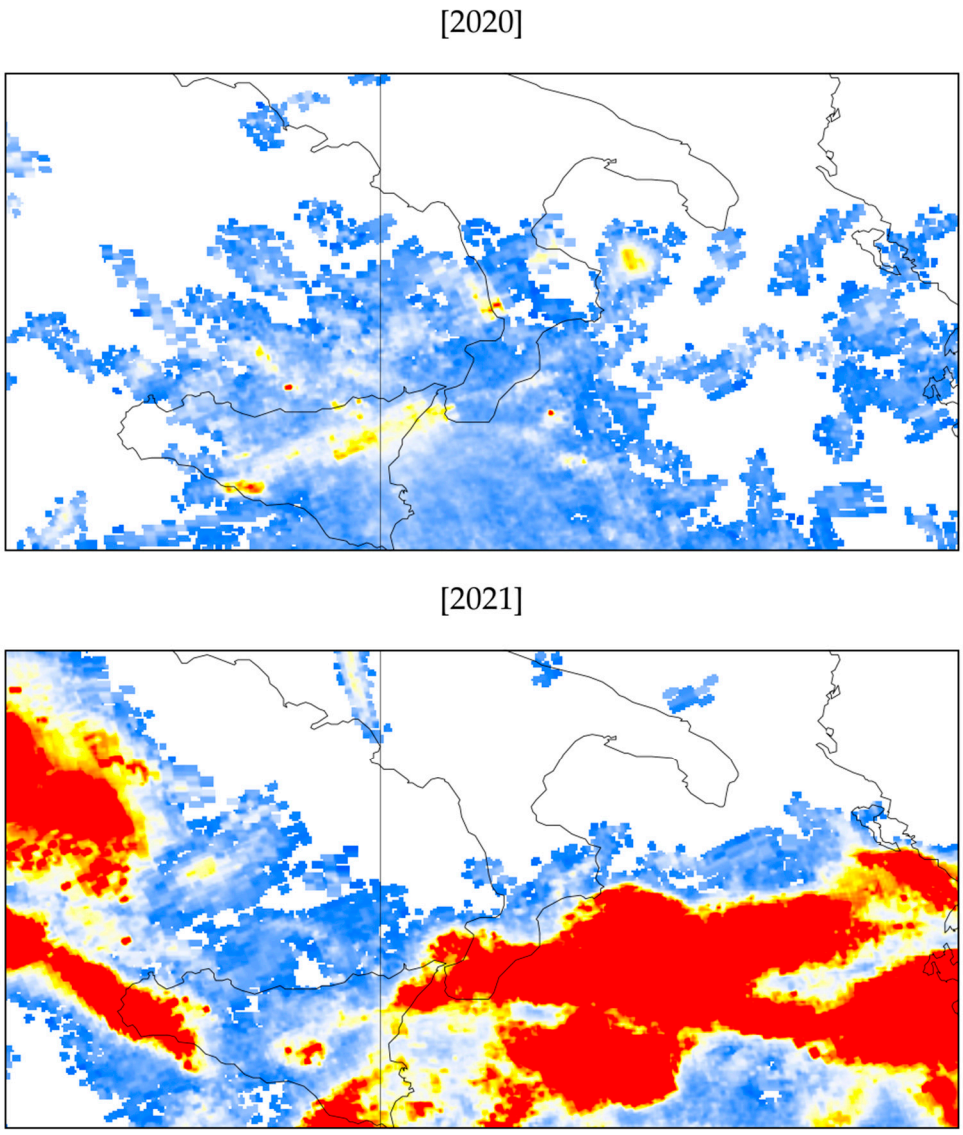

Figure 9. *Cont.*

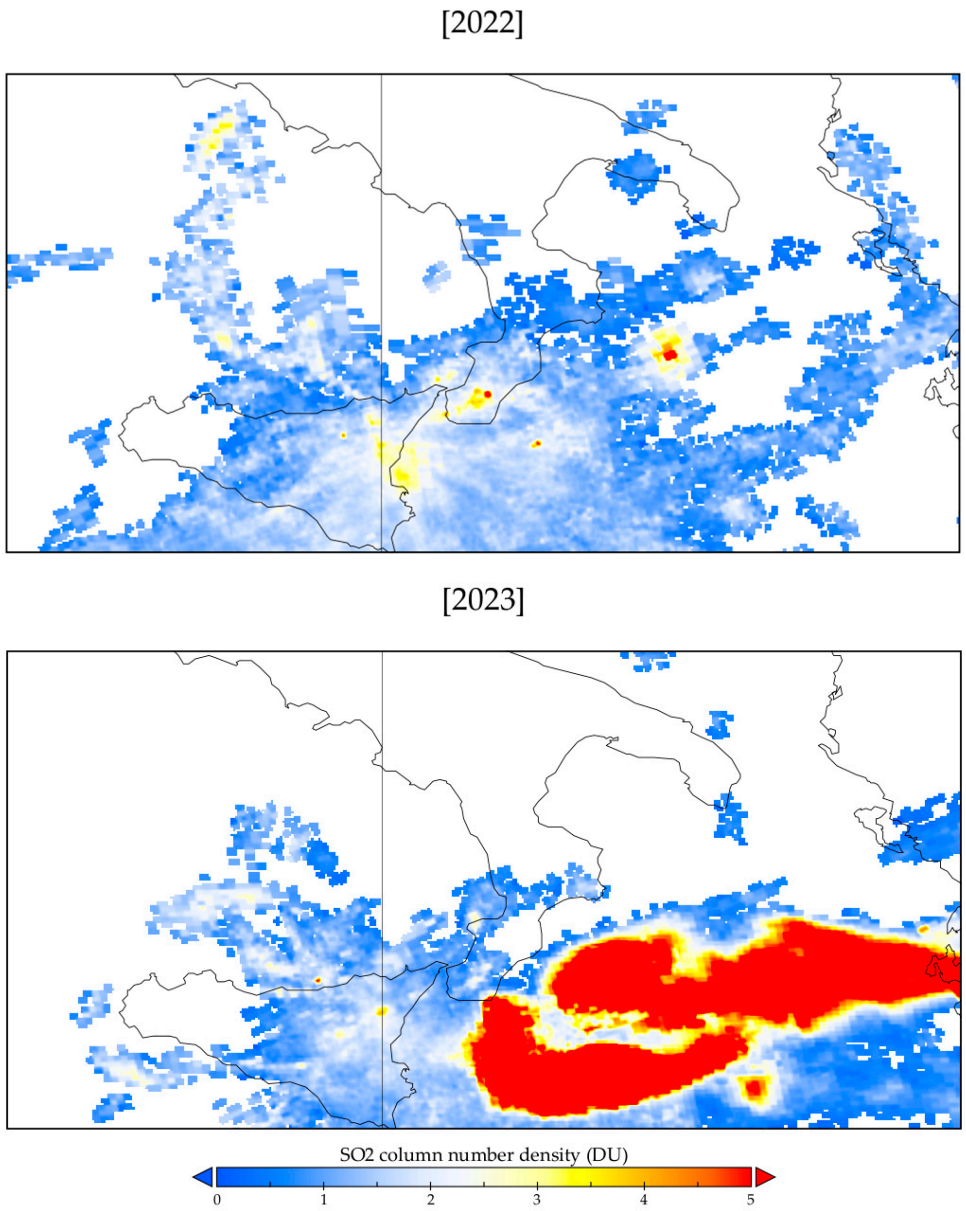

Figure 9. SO_2 column number density (DU) for 2020–2023 created using COBRA.

COBRA-derived SO_2 column data for volcanic eruptions were calculated for three different assumed plume height thresholds: 15, 7, and 2.5 km. The advantage of COBRA is its capacity to reveal and pinpoint weak sources of SO_2 that are not normally detected with TROPOMIs; plotted data are reported to be more susceptible to the 7 km altitude threshold. The maps clearly indicate the presence of relevant natural sources of SO_2 in southern Italy, i.e., volcanoes.

4. Discussion

At the Lamezia Terme (LMT) WMO/GAW station, a multi-year and cyclic characterization of sulfur dioxide (SO_2) was performed based on 2016–2023 surface data gathered at the observation site. SO_2 is the third parameter subjected to such a data evaluation, following methane [78] and ozone [79]. Due to SO_2's heterogeneous sources and the presence of a volcanic arc less than 100 km from the observatory (Figure 1), this study integrated the analysis of TROPOMI data on tropospheric column densities gathered by Sentinel-5P between 2020 and 2023. Specifically, a number of target coordinates were designated as representative of

the Tyrrhenian and Ionian coasts of central Calabria, with three points (TYR1–3) specifically selected in proximity of the nearest active volcano, Stromboli (Figure 2). This is the first occurrence of an integrated analysis of surface and satellite data at the LMT based on a medium-term data series.

In the analysis of daily cycles of SO_2 at the site, an early morning peak (greater than 1.2 ppb) is observed between 09:00 and 16:00. Two minor peaks in the 0.3 ppb range match rush hour traffic hours. These findings are in accordance with those of Cristofanelli et al. (2017) [93], who first assessed the influence of vehicular traffic at the site based on the analysis of other pollutants, and those of D'Amico et al. (2024c) [94], who compared 2020 COVID-19 lockdown period data with the pre- and post-lockdown peaks to show the differences caused by exceptionally low anthropic activities. The daily cycle of SO_2 at the LMT is characterized by a 12:00 h peak that matches the peak in sea breezes and is compatible with the transport of air masses from the west. This pattern is similar to that observed for surface ozone at the LMT [79] but is narrowed down to a shorter time window. The influence of solar radiation and, in particular, local wind circulation is well documented in Figure 3C, where the observed peaks are differentiated by wind corridor.

In the context of the Mediterranean basin, the relationship between gases present in the atmosphere, temperatures, and solar radiation has been the subject of research. In the case of ozone [120,121], research studies have found evidence of different patterns between the eastern and western Mediterranean sectors. At the LMT, the complexities in the distribution of gases and aerosols are amplified by the contribution of anthropogenic sources and, with respect to SO_2, by the presence of a volcanic arc and a major volcano in a 160 km radius from the observation site. The Mediterranean is recognized as a hotspot for air quality [122] and an intersection for several distinct air mass transport processes [123–125]. For this reason, a precise understanding of the mechanisms driving changes in the observed cycles and trends is necessary.

The correlations between SO_2 concentrations and wind data shown in Figures 4 and 5 also indicate the presence of westerly peaks compatible with possible volcanic and shipping emissions. Many of the SO_2 peaks occur at high wind speeds, which indicate air mass transport from the Tyrrhenian Sea and is likely not related to local emissions in the context of the Calabrian peninsula.

In detail, from the western sectors, SO_2 concentrations reach peaks above 3.4 ppb, both in the case of winds below 5 m/s (breeze regimes) and in synoptic conditions with speeds that can exceed the 8 m/s threshold. From the northeastern sector, winter and fall concentrations are linked to values that exceed the 5 ppb threshold under both breeze regimes and synoptic conditions where wind speeds exceed 7–8 m/s. These patterns affecting cold seasons are compatible with anthropogenic emissions from fossil fuels in nearby urban areas. Wind regimes were found in a 2024 campaign integrating greenhouse gas, aerosol, and planetary boundary layer (PBL) data to influence several parameters at the LMT [104]. The differentiation between two corridors remains one of the main characteristics of the LMT.

Under the assumption that only anthropogenic emissions are subject to weekly cycles, unlike natural emissions, which are not affected [100], weekly assessments of SO_2 concentrations were performed. For the first time in the history of LMT observations, a weekly analysis was also applied to tropospheric column data. In Figure 6, surface fluctuations are linked to winter peaks falling outside weekends, a pattern that may be compatible with anthropogenic emissions, although further investigations would be required. Tropospheric column data reported in Figure 6 are also subject to weekly oscillations, but the TYR points are less affected; this is compatible with natural emissions and could therefore point to volcanic activity (in the form of fumarole and constant gaseous outputs) as responsible for

these regular patterns that are not seen at the LMT and ION due to increased anthropogenic influence. Maritime shipping due to the Gioia Tauro port located on the Tyrrhenian coast of Calabria could also be responsible for the TYR and LMT baseline values higher than those of ION.

The multi-year variability of surface SO_2 was evaluated, and the results are shown in Figure 7. For the first time in the history of the LMT, a multi-year evaluation (2020–2023) was also applied to tropospheric column data, and the results are shown in Figure 8.

By differentiating surface SO_2 averages by wind corridor (Figure 7), higher concentrations linked to westerly winds are prominent and are compatible with maritime shipping and volcanic activity. The implementation and evaluation of TROPOMI data (Figure 8), aimed at the TYR1–4 points in the Tyrrhenian Sea and the ION1 point in the Ionian Sea, in conjunction with tropospheric column data on the LMT site itself, constitute a completely new methodology for the assessment of local observations. The LMT's surface and column data (Figure 8C) are mostly in accordance, peaks included.

A comparison between TYR4 and ION1 was performed to assess coast-to-coast differences in tropospheric column data in the narrowest point of the entire Italian peninsula (≈32 km between the two coasts) (Figure 2), in an area characterized by the presence of the Marcellinara Gap as one of the orographic factors channeling wind circulation between the two seas [95,96]. The graph shows that TYR4, representative of near-shore Tyrrhenian conditions, yields generally higher values compared to ION1, which is its Ionian counterpart. In Figure 8D, the TYR1–3 points—which are further away from the Tyrrhenian coast—are analyzed in detail to highlight contributions from volcanic activity. The results indicate that the three points are not affected in the same way, with the southernmost location (TYR1) generally yielding much lower density values compared to the central (TYR2) and northern (TYR3) points. It is worth mentioning that TYR2 is closer to Stromboli than TYR1 by approximately 1.5 km, especially when considering the volcanic cone and *Sciara del Fuoco*, which is the southwestern slope of the volcano along which most lava flows occur [87,88]. Due to the characteristics of prevailing large-scale circulation [95] from the west, a Stromboli–TYR2-TYR4-LMT path is compatible with reported observations and TYR2's higher SO_2 values, while the Stromboli–TYR1-TYR4-LMT path would be less dependent on that. With Vulcano's activity being mostly limited to fumarole, TYR1's shorter distance to the second volcano is likely not a key factor.

In addition to the plots and graphs of surface and satellite data, statistical evaluations were performed in Section 3.5 to test possible correlations between a number of parameters. As shown in Table 3 (2016–2023), the mean temperature (17.78 °C) is higher than the median (17.21 °C). This suggests a slight positive skew in the data, with more temperature values falling below the mean. However, the difference still indicates a roughly symmetrical distribution with a slight tendency toward warmer temperatures. The first quartile is 13.38 °C, and the third is 22.66 °C. This indicates that half of the data fall between these temperatures, reflecting the range of conditions experienced during this period. Similarly, SO_2's mean value is 0.217 ppb with a third quartile threshold of 0.142 ppb, indicating a right skew in the data. This means that the majority of SO_2 measurements are in the low range, but there are sporadic high concentrations driving the mean upward. These conditions are representative of a "multisource" observation site where low background values of a parameter are affected by perturbances.

RH also shows evidence of skewness: the mean is 67.44%, which is slightly lower than the median (68.9%). Overall, there is considerable variability in the data of each parameter: air temperature and RH have moderate standard deviations, while SO_2 and wind speed (WS) show wider spreads, suggesting that these variables fluctuate more.

With respect to statistical correlations, surface data (2016–2023) were evaluated, with the results shown in Table 4. From the analysis, which also relied on Pearson's Correlation Coefficient (PCC) and Spearman's Rank Correlation Coefficient (SR), it is possible to determine that there is virtually no linear correlation between air temperature and SO_2 mole fractions measured at the site; in particular, the PCC is close to zero. All *p*-values in Table 4 are lower than 0.001, except, in fact, for SO_2/T at 0.89. The SR of the relationship is 0.096 with a significance of <0.001, which is still insufficient to indicate a solid linear correlation. A weak but statistically relevant correlation is observed between SO_2 and RH, especially for the SR (−0.26), while the PPC is very low at 0.038. Overall, no clear correlations emerge in the evaluation; the absence of a correlation between SO_2 and air temperature has environmental implications due to the temperature's variability between boreal warm and cold seasons.

Possible correlations between surface and tropospheric column SO_2 (Table 5), limited to the 2020–2023 period, are evaluated in Table 6. In the correlation matrix, both PCC (0.042) and the SR (0.085) indicate a weak correlation between surface and TVC data, with the SR showing a statistically significant *p*-value below the 0.5 threshold. These results have a number of possible explanations: Bias errors in satellite data processing algorithms may have had a role; however, it is possible to justify this with the coexistence of near-surface anthropogenic pollution such as maritime shipping and volcanic outputs, which are subject to different transport mechanisms. The outputs of volcanic eruptions from the Aeolian Arc, as well as Mount Etna, reach high altitudes and are therefore subject to transport over a large area: if these outputs pass above the LMT at sufficiently high altitudes, peaks in the TVC data will lack a surface counterpart.

The findings based on the implementation of the TYR and ION locations were further evaluated via satellite products on SO_2 emissions over a large area. TROPOMI products are used in the literature to provide estimates on SO_2 emissions from a range of sources [126]; however, they may have been subject to artifacts. With the COvariance-Based Retrieval Algorithm (COBRA), Level 3 products can be used to generate maps that partially compensate for some of the issues affecting regular evaluations [115,116]. In Figure 9, maps showing the multi-year variability of SO_2 column number densities provide a large-scale picture of natural SO_2 emissions in the area. In fact, large-scale wind circulation has a dominant westerly nature [95], and this leads to prevailing transport toward the east of volcanic outputs such as those attributable to Mount Etna in Sicily.

Overall, the findings described in this study set up new fundaments and methodologies upon which future assessments of SO_2 in the area could be performed to discriminate natural and anthropogenic sources. Additional methodologies such as the carbon isotope fractionation of carbon dioxide (δ^{13}C-CO_2) [127], which is also a product of volcanic activity, could be used in source apportionment: the characteristic isotopic fingerprint of volcanic carbon dioxide (CO_2), paired with surface observations of SO_2, could differentiate volcanic and anthropogenic sources [128–131] and thus provide a clear understanding of volcanic influence over LMT observations. With the PSCF (Potential Source Contribution Function) [132–134] and/or CWT (Concentration Weighted Trajectory) [135–138], case studies could also be subject to further research to provide additional details and insights on the contribution of natural and anthropogenic SO_2 emissions to LMT measurements.

5. Conclusions

Through the implementation of new methodologies that have never been applied to similar studies at the same observation site, integrated surface and tropospheric column data on sulfur dioxide (SO_2) were evaluated at the Lamezia Terme (code: LMT) WMO/GAW station in Calabria, Southern Italy.

Surface (2016–2023) and satellite (2020–2023) data provided new evidence of possible volcanic activity influence over LMT measurements due to the presence of the Aeolian Arc and Mount Etna in a 160 km radius from the station. Surface measurements, in conjunction with satellite data on select coordinates within the Tyrrhenian and Ionian seas, indicate that SO_2 peaks are linked to westerly winds compatible with maritime shipping and volcanic pollution. The target coordinates selected for satellite data evaluations are based on local wind circulation, which is known to be characterized by a western–seaside sector and a northeastern–continental sector. Local wind circulation and air mass transport is subject to winds alternating between these sectors. The findings seem to indicate that volcanic outputs from the Aeolian Arc are subject to westerly winds, which may drive air mass transport toward the LMT observation site. Maps generated from cumulative yearly Level 3 satellite observations—processed by COBRA and meant to compensate for TROPOMI artifacts—also show the presence of multiple sources of the SO_2 in the area and a dominating westerly flow that contributes to the transport of volcanic outputs, especially those attributable to Mount Etna in Sicily.

SO_2 peaks linked to westerly winds from the Tyrrhenian Sea are in contrast with other observed trends at the same site, where northeastern–continental winds are generally enriched in pollutants, while western–seaside winds generally yield low concentrations of compounds attributable to anthropic activity. SO_2 variability at the site is also distinct from that of surface ozone, a compound that shares similar patterns but shows different seasonal and diurnal trends. At the LMT, higher SO_2 concentrations are also observed in the case of synoptic conditions where wind speeds exceed the thresholds of 7–8 m/s, thus indicating the influence of air mass transport from other locations.

This research study sets new fundaments upon which future source apportionment efforts could be based on. Through the implementation of additional methodologies, the influence of volcanic activity on LMT measurements could be assessed with greater detail, thus providing new insights on the role played by active volcanoes in air mass transport within the context of a climatic hotspot such as the Mediterranean basin. Furthermore, this study shows the importance of performing multi-year evaluations of specific compounds to assess their cycles, variability, and trends with enhanced detail.

Supplementary Materials: The following supporting information can be downloaded at https://www.mdpi.com/article/10.3390/environments12010027/s1: TBFIL. Figure S1: Seasonal wind rose scatter plots of SO_2 at LMT, divided by year (2016–2023); Figure S2-A1–S2-H3: Correlations between wind speeds and SO_2 mole fractions, divided by sector and referring to the entire observation period (2016–2023); Figure S3-A1–S3-H3: Weekly distribution of SO_2 averages, divided by sector and referring to the entire observation period (2016–2023).

Author Contributions: Conceptualization, F.D., T.L.F. and C.R.C.; methodology, F.D., T.L.F., D.G. and C.R.C.; software, F.D., T.L.F., D.G., S.S. and G.D.B.; validation, T.L.F., D.G., I.A. and C.R.C.; formal analysis, F.D., T.L.F. and D.G.; investigation, F.D., T.L.F. and D.G.; data curation, F.D., T.L.F., D.G., I.A., L.M., S.S., G.D.B. and C.R.C.; writing—original draft preparation, F.D. and T.L.F.; writing—review and editing, F.D., T.L.F., D.G., I.A., M.D.P., L.M., S.S., G.D.B. and C.R.C.; visualization, F.D., T.L.F., D.G., L.M., S.S. and G.D.B.; supervision, C.R.C.; funding acquisition, C.R.C. and M.D.P. All authors have read and agreed to the published version of the manuscript.

Funding: This research was funded by AIR0000032—ITINERIS, the Italian Integrated Environmental Research Infrastructures System (D.D. n. 130/2022—CUP B53C22002150006) under the EU—Next Generation EU PNRR—Mission 4 "Education and Research"—Component 2: "From research to business"—Investment 3.1: "Fund for the realization of an integrated system of research and innovation infrastructures".

Data Availability Statement: The surface datasets presented in this article are not readily available because they are part of other ongoing studies.

Acknowledgments: The authors would like to acknowledge the support of the editor and also thank the three anonymous reviewers who contributed to significantly improve and expand the manuscript.

Conflicts of Interest: The authors declare no conflicts of interest.

References

1. Eriksson, E. The yearly circulation of sulfur in nature. *J. Geophys. Res.* **1963**, *68*, 4001–4008. [CrossRef]
2. Robinson, E.; Robbins, R.C. Gaseous sulfur pollutants from urban and natural sources. *J. Air Pollut. Control Assoc.* **1970**, *20*, 233–235. [CrossRef]
3. Feinberg, A.; Sukhodolov, T.; Luo, B.-P.; Rozanov, E.; Winkel, L.H.E.; Peter, T.; Stenke, A. Imrpoved tropospheric and stratospheric sulfur cycle in the aerosol-chemistry-climate model SOCOL-AERv2. *Geosci. Model. Dev.* **2019**, *12*, 3863–3887. [CrossRef]
4. Brodowsky, C.V.; Sukhodolov, T.; Chiodo, G.; Aquila, V.; Bekki, S.; Dhomse, S.S.; Hopfner, M.; Laakso, A.; Mann, G.W.; Niemeier, U.; et al. Analysis of the global atmospheric background sulfur budget in a multi-model framework. *Atmos. Chem. Phys.* **2024**, *24*, 5513–5548. [CrossRef]
5. Berresheim, H.; Jaeschke, W. The contribution of volcanoes to the global atmospheric sulfur budget. *J. Geophys. Res.-Oceans* **1983**, *88*, 3732–3740. [CrossRef]
6. Bhugwant, C.; Siéja, B.; Bessafi, M.; Staudacher, T.; Ecormier, J. Atmospheric sulfur dioxide measurements during the 2005 and 2007 eruptions of the Piton de La Fournaise volcano: Implications for human health and environmental changes. *J. Volcanol. Geotherm. Res.* **2009**, *184*, 208–224. [CrossRef]
7. Mills, M.J.; Schmidt, A.; Easter, R.; Solomon, S.; Kinnison, D.E.; Ghan, S.J.; Neely, R.R., III; Marsh, D.R.; Conley, A.; Bardeen, C.G.; et al. Global volcanic aerosol properties derived from emissions, 1990–2014, using CESM1(WACCM). *J. Geophys. Res.–Atmos.* **2016**, *121*, 2332–2348. [CrossRef]
8. Filippi, J.-B.; Durand, J.; Tulet, P.; Bielli, S. Multiscale Modeling of Convection and Pollutant Transport Associated with Volcanic Eruption and Lava Flow: Application to the April 2007 Eruption of the Piton de la Fournaise (Reunion Island). *Atmosphere* **2021**, *12*, 507. [CrossRef]
9. Cadle, R.D. Volcanic emissions of halides and sulfur compounds to the troposphere and stratosphere. *J. Geophys. Res.-Oceans* **1975**, *80*, 1650–1652. [CrossRef]
10. Bluth, G.J.S.; Schnetzler, C.C.; Krueger, A.J.; Walter, L.S. The contribution of explosive volcanism to global atmospheric sulphur dioxide concentrations. *Nature* **1993**, *366*, 327–329. [CrossRef]
11. Ge, C.; Wang, J.; Carn, S.; Yang, K.; Ginoux, P.; Krotkov, N. Satellite-based global volcanic SO_2 emissions and sulfate direct radiative forcing during 2005–2012. *J. Geophys. Res.–Atmos.* **2016**, *121*, 3446–3464. [CrossRef]
12. Schmidt, A.; Mills, M.J.; Ghan, S.; Gregory, J.M.; Allan, R.P.; Andrews, T.; Bardeen, C.G.; Conley, A.; Forster, P.M.; Gettelman, A.; et al. Volcanic radiative forcing from 1979 to 2015. *J. Geophys. Res.–Atmos.* **2018**, *123*, 12491–12508. [CrossRef]
13. Bluth, G.J.S.; Doiron, S.D.; Schnetzler, C.C.; Krueger, A.J.; Walter, L.S. Global tracking of the SO_2 clouds from the June, 1991 Mount Pinatubo eruptions. *Geophys. Res. Lett.* **1992**, *19*, 151–154. [CrossRef]
14. Mankin, W.G.; Coffey, M.T.; Goldman, A. Airborne observations of SO_2, HCl, and O_3 in the stratospheric plume of the Pinatubo Volcano in July 1992. *Geophys. Res. Lett.* **1992**, *19*, 179–182. [CrossRef]
15. Goldman, A.; Murcray, F.J.; Rinsland, C.P.; Blatherwick, R.D.; David, S.J.; Murcray, F.H.; Murcray, D.G.M. Pinatubo SO_2 column measurements from Mauna Loa. *Geophys. Res. Lett.* **1992**, *19*, 183–186. [CrossRef]
16. Baran, A.J.; Foot, J.S.; Dibben, P.C. Satellite detection of volcanic sulphuric acid aerosol. *Geophys. Res. Lett.* **1993**, *20*, 1799–1801. [CrossRef]
17. Guo, S.; Bluth, G.J.S.; Rose, W.I.; Watson, I.M.; Prata, A.J. Re-evaluation of SO_2 release of the 15 June 1991 Pinatubo eruption using ultraviolet and infrared satellite sensors. *Geochem. Geophys. Geosyst.* **2004**, *5*, Q04001. [CrossRef]
18. Mishra, M.K.; Hoffmann, L.; Thapliyal, P.K. Investigations on the Global Spread of the Hunga Tonga-Hunga Ha'apai Volcanic Eruption Using Space-Based Observations and Lagrangian Transport Simulations. *Atmosphere* **2022**, *13*, 2055. [CrossRef]
19. Sun, Q.; Lu, T.; Li, D.; Xu, J. The Impact of the Hunga Tonga–Hunga Ha'apai Volcanic Eruption on the Stratospheric Environment. *Atmosphere* **2024**, *15*, 483. [CrossRef]
20. Clinton, N.E.; Gong, P.; Scott, K. Quantification of pollutants emitted from very large wildland fires in Southern California, USA. *Atmos. Environ.* **2006**, *40*, 3686–3695. [CrossRef]
21. Granier, C.; Bessagnet, B.; Bond, T.; D'Angiola, A.; Denier van der Gon, H.; Frost, G.J.; Heil, A.; Kaiser, J.W.; Kinne, S.; Klimont, Z.; et al. Evolution of anthropogenic and biomass burning emissions of air pollutants at global and regional scales during the 1980–2010 period. *Clim. Chang.* **2011**, *109*, 163. [CrossRef]
22. Urbanski, S. Wildland fire emissions, carbon, and climate: Emission factors. *For. Ecol. Manag.* **2014**, *317*, 51–60. [CrossRef]

23. He, C.; Miljevic, B.; Crilley, L.R.; Surawski, N.C.; Bartsch, J.; Salimi, F.; Uhde, E.; Schnelle-Kreis, J.; Orasche, J.; Ristovski, Z.; et al. Characterisation of the impact of open biomass burning on urban air quality in Brisbane, Australia. *Environ. Int.* **2016**, *91*, 230–242. [CrossRef]
24. Rickly, P.S.; Guo, H.; Campuzano-Jost, P.; Jimenez, J.L.; Wolfe, G.M.; Bennett, R.; Bourgeois, I.; Crounse, J.D.; Dibb, J.E.; DiGangi, J.P.; et al. Emission factors and evolution of SO_2 measured from biomass burning in wildfires and agricultural fires. *Atmos. Chem. Phys.* **2022**, *22*, 15603–15620. [CrossRef]
25. Ning, X.; Li, J.; Zhuang, P.; Lai, S.; Zheng, X. Wildfire combustion emission inventory in Southwest China (2001-2020) based on MODIS fire radiative energy data. *Atmos. Pollut. Res.* **2024**, *15*, 102279. [CrossRef]
26. Rollins, A.W.; Thornberry, T.D.; Watts, L.A.; Yu, P.; Rosenlof, K.H.; Mills, M.; Baumann, E.; Giorgetta, F.R.; Bui, T.V.; Höpfner, M.; et al. The role of sulfur dioxide in stratospheric aerosol formation evaluated by using in situ measurements in the tropical lower stratosphere. *Geophys. Res. Lett.* **2017**, *44*, 4280–4286. [CrossRef]
27. Guzewich, S.D.; Oman, L.D.; Richardson, J.A.; Whelley, P.L.; Bastelberger, S.T.; Young, K.E.; Bleacher, J.E.; Fauchez, T.J.; Kopparapu, R.K. Volcanic Climate Warming Through Radiative and Dynamical Feedbacks of SO2 Emissions. *Geophys. Res. Lett.* **2022**, *49*, e2021GL096612. [CrossRef]
28. Yu, P.; Portmann, R.W.; Peng, Y.; Liu, C.-C.; Zhu, Y.; Asher, E.; Bai, Z.; Lu, Y.; Bian, J.; Mills, M.; et al. Radiative forcing from the 2024–2022 volcanic and wildfire injections. *Geophys. Res. Lett.* **2023**, *50*, e2023GL103791. [CrossRef]
29. Sheng, J.-X.; Weisenstein, D.K.; Luo, B.-P.; Rozanov, E.; Stenke, A.; Anet, J.; Bingemer, H.; Peter, T. Global atmospheric sulfur budget under volcanically quiescent conditions: Aerosol-chemistry-climate model predictions and validation. *J. Geophys. Res.-Atmos.* **2015**, *120*, 256–276. [CrossRef]
30. Klimont, Z.; Smith, S.J.; Cofala, J. The last decade of global anthropogenic sulfur dioxide: 2000–11 emissions. *Environ. Res. Lett.* **2013**, *8*, 014003. [CrossRef]
31. Asghar, U.; Rafiq, S.; Anwar, A.; Iqbal, T.; Ahmed, A.; Jamil, F.; Khurram, M.S.; Akbar, M.M.; Farooq, A.; Shah, N.S.; et al. Review on the progress in emission control technologies for the abatement of CO_2, SO_x and NO_x from fuel combustion. *J. Environ. Chem. Eng.* **2021**, *9*, 106064. [CrossRef]
32. Fukusaki, Y.; Umehara, M.; Kousa, Y.; Inomata, Y.; Nakai, S. Investigation of Air Pollutants Related to the Vehicular Exhaust Emissions in the Kathmandu Valley, Nepal. *Atmosphere* **2021**, *12*, 1322. [CrossRef]
33. Wallington, T.J.; Anderson, J.E.; Dolan, R.H.; Winkler, S.L. Vehicle Emissions and Urban Air Quality: 60 Years of Progress. *Atmosphere* **2022**, *13*, 650. [CrossRef]
34. McDonald-Buller, E.; McGaughey, G.; Grant, J.; Shah, T.; Kimura, Y.; Yarwood, G. Emissions and Air Quality Implications of Upstream and Midstream Oil and Gas Operations in Mexico. *Atmosphere* **2021**, *12*, 1696. [CrossRef]
35. Abdul-Wahab, S.; Ali, S.; Sardar, S.; Irfan, N. Impacts on Ambient Air Quality Due to Flaring Activities in One of Oman's Oilfields. *Arch. Environ. Occup. Health* **2012**, *67*, 3–14. [CrossRef]
36. Dore, A.; Vieno, M.; Tang, Y.; Dragosits, U.; Dosio, A.; Weston, K.; Sutton, M. Modelling the atmospheric transport and deposition of sulphur and nitrogen over the United Kingdom and assessment of the influence of SO_2 emissions from international shipping. *Atmos. Environ.* **2007**, *41*, 2355–2367. [CrossRef]
37. Berg, N.; Mellqvist, J.; Jalkanen, J.-P.; Balzani, J. Ship emissions of SO_2 and NO_2: DOAS measurements from airborne platforms. *Atmos. Meas. Tech.* **2012**, *5*, 1085–1098. [CrossRef]
38. Spengler, T.; Tovar, B. Environmental Valuation of In-Port Shipping Emissions per Shipping Sector on Four Spanish Ports. *Mar. Pollut. Bull.* **2022**, *178*, 113589. [CrossRef] [PubMed]
39. Fuentes García, G.; Echeverría, R.S.; Reynoso, A.G.; Baldasano Recio, J.M.; Rueda, V.M.; Retama Hernández, A.; Kahl, J.D.W. Sea Port SO_2 Atmospheric Emissions Influence on Air Quality and Exposure at Veracruz, Mexico. *Atmosphere* **2022**, *13*, 1950. [CrossRef]
40. Gamal, G.; Abdeldayem, O.M.; Elattar, H.; Hendy, S.; Gabr, M.E.; Mostafa, M.K. Remote Sensing Surveillance of NO_2, SO_2, CO, and AOD along the Suez Canal Pre- and Post-COVID-19 Lockdown Periods and during the Blockage. *Sustainability* **2023**, *15*, 9362. [CrossRef]
41. Paternina-Arboleda, C.D.; Agudelo-Castañeda, D.; Voß, S.; Das, S. Towards Cleaner Ports: Predictive Modeling of Sulfur Dioxide Shipping Emissions in Maritime Facilities Using Machine Learning. *Sustainability* **2023**, *15*, 12171. [CrossRef]
42. Ballini, F.; Bozzo, R. Air Pollution from Ships in Ports: The Socio-Economic Benefit of Cold-Ironing Technology. *Res. Transp. Bus. Manag.* **2015**, *17*, 92–98. [CrossRef]
43. Isakson, J.; Persson, T.A.; Lindgren, E.S. Identification and assessment of ship emissions and their effects in the harbour of Göteborg, Sweden. *Atmos. Environ.* **2001**, *35*, 3659–3666. [CrossRef]
44. Anastasopolos, A.T.; Sofowote, U.M.; Hopke, P.K.; Rouleau, M.; Shin, T.; Dheri, A.; Peng, H.; Kulka, R.; Gibson, M.D.; Farah, P.-M.; et al. Air quality in Canadian port cities after regulation of low-sulphur marine fuel in the North American Emissions Control Area. *Sci. Total Environ.* **2021**, *791*, 147949. [CrossRef] [PubMed]

45. Miake-Lye, R.C.; Anderson, B.E.; Cofer, W.R.; Wallio, H.A.; Nowicki, G.D.; Ballenthin, J.O.; Hunton, D.E.; Knighton, W.B.; Miller, T.M.; Seeley, J.V.; et al. SO_x oxidation and volatile aerosol in aircraft exhaust plumes depend on fuel sulfur content. *Geophys. Res. Lett.* **1998**, *25*, 1677–1680. [CrossRef]
46. Fan, W.; Sun, Y.; Zhu, T.; Wen, Y. Emissions of HC, CO, NO_x, CO_2, and SO_2 from civil aviation in China in 2010. *Atmos. Environ.* **2012**, *56*, 52–57. [CrossRef]
47. Zhou, Y.; Jiao, Y.; Lang, J.; Chen, D.; Huang, C.; Wei, P.; Li, S.; Cheng, S. Improved estimation of air pollutant emissions from landing and takeoff cycles of civil aircraft in China. *Environ. Pollut.* **2019**, *249*, 463–471. [CrossRef]
48. Kärcher, B.; Hirschberg, M.; Fabian, P. Small-scale chemical evolution of aircraft exhaust species at cruising altitudes. *J. Geophys. Res.-Atmos.* **1996**, *101*, 15169–15190. [CrossRef]
49. An, H.; Wang, Y.; Wang, Y.; Liu, J.; Tang, X.; Yi, H. Civil aviation emissions in China in 2019: Characteristics and abatement potential. *J. Environ. Sci.* **2025**, *151*, 225–237. [CrossRef]
50. Schumann, U.; Arnold, F.; Busen, R.; Curtius, J.; Kärcher, B.; Kiendler, A.; Petzold, A.; Schlager, H.; Schröder, F.; Wohlfrom, K.-H. Influence of fuel sulfur on the composition of aircraft exhaust plumes: The experiments SULFUR 1–7. *J. Geophys. Res.-Atmos.* **2002**, *107*, AAC 2-1–AAC 2-27. [CrossRef]
51. Voitsekhovskaya, O.K.; Kashirskii, D.E.; Egorov, O.V. Spectroscopic support of laser remote sensing of the sulfur dioxide gas in the jet of engine exhaust gases. *Russ. Phys. J.* **2013**, *56*, 473–482. [CrossRef]
52. Dischl, R.; Sauer, D.; Voigt, C.; Harlaß, T.; Sakellariou, F.; Märkl, R.; Schumann, U.; Scheibe, M.; Kaufmann, S.; Roiger, A.; et al. Measurements of particle emissions of an A350-941 burning 100% sustainable aviation fuels in cruise. *Atmos. Chem. Phys.* **2024**, *24*, 11255–11273. [CrossRef]
53. Meetham, A.R. Natural removal of pollution from the atmosphere. *Q. J. R. Meteorol. Soc.* **1950**, *76*, 359–371. [CrossRef]
54. Rodhe, H. Budgets and turn-over times of atmospheric sulfur compounds. *Atmos. Environ.* **1978**, *12*, 671–680. [CrossRef]
55. Lee, C.; Martin, R.V.; van Donkelaar, A.; Lee, H.; Dickerson, R.R.; Hains, J.C.; Krotkov, N.; Richter, A.; Vinnikov, K.; Schwab, J.J. SO_2 emissions and lifetimes: Estimates from inverse modeling using in situ and global, space-based (SCIAMACHY and OMI) observations. *J. Geophys. Res.–Atmos.* **2011**, *116*, D06304. [CrossRef]
56. Renuka, K.; Gadhavi, H.; Jayaraman, A.; Bhaskara Rao, S.V.; Lal, S. Study of mixing ratios of SO_2 in a tropical rural environment in south India. *J. Earth Syst. Sci.* **2020**, *129*, 104. [CrossRef]
57. Garland, J.A. Dry and wet removal of sulphur from the atmosphere. *Atmos. Environ.* **1978**, *12*, 349–362. [CrossRef]
58. Charlson, R.; Lovelock, J.; Andreae, M.; Warren, S.G. Oceanic phytoplankton, atmospheric sulphur, cloud albedo and climate. *Nature* **1987**, *326*, 655–661. [CrossRef]
59. Khan, R.R.; Siddiqui, M. Review on effects of particulates; sulfur dioxide and nitrogen dioxide on human health. *Int. Res. J. Environ. Sci.* **2014**, *3*, 70–73.
60. Greenberg, N.; Carel, R.S.; Derazne, E.; Tiktinsky, A.; Tzur, D.; Portnov, B.A. Modeling long-term effects attributed to nitrogen dioxide (NO_2) and sulfur dioxide (SO_2) exposure on asthma morbidity in a nationwide cohort in Israel. *J. Toxicol. Environ. Health* **2017**, *80*, 326–337. [CrossRef] [PubMed]
61. Szyszkowicz, M. Air pollution and emergency department visits for depression in Edmonton, Canada. *Int. J. Occup. Med. Environ. Health* **2007**, *20*, 241–245. [CrossRef] [PubMed]
62. Shin, J.; Park, J.Y.; Choi, J. Long-term exposure to ambient air pollutants and mental health status: A nationwide population-based cross-sectional study. *PLoS ONE* **2018**, *13*, e0195607. [CrossRef] [PubMed]
63. Lelieveld, J.; Evans, J.S.; Fnais, M.; Giannadaki, D.; Pozzer, A. The contribution of outdoor air pollution sources to premature mortality on a global scale. *Nature* **2015**, *525*, 367–371. [CrossRef]
64. Hemminki, K.; Niemi, M.L. Community study of spontaneous abortions: Relation to occupation and air pollution by sulfur dioxide, hydrogen sulfide, and carbon disulfide. *Int. Arch. Occup. Environ. Health* **1982**, *51*, 55–63. [CrossRef] [PubMed]
65. Xu, X.; Ding, H.; Wang, X. Acute effects of total suspended particles and sulfur dioxides on preterm delivery: A community-based cohort study. *Arch. Environ. Health* **1995**, *50*, 407–415. [CrossRef] [PubMed]
66. Lin, C.; Li, C.; Yang, G.; Mao, I. Association between maternal exposure to elevated ambient sulfur dioxide during pregnancy and term low birth weight. *Environ. Res.* **2004**, *96*, 41–50. [CrossRef] [PubMed]
67. Enkhmaa, D.; Warburton, N.; Javzandulam, B.; Uyanga, J.; Khishigsuren, Y.; Lodoysamba, S.; Enkhtur, S.; Warburton, D. Seasonal ambient air pollution correlates strongly with spontaneous abortion in Mongolia. *BMC Pregnancy Childbirth* **2014**, *14*, 146. [CrossRef] [PubMed]
68. Smith, S.J.; van Aardenne, J.; Klimont, Z.; Andres, R.J.; Volke, A.; Arias, S.D. Anthropogenic sulfur dioxide emissions: 1850–2005. *Atmos. Chem. Phys.* **2011**, *11*, 1101–1116. [CrossRef]
69. Zhou, Z.; Ye, X.; Ge, X. The Impacts of Technical Progress on Sulfur Dioxide Kuznets Curve in China: A Spatial Panel Data Approach. *Sustainability* **2017**, *9*, 674. [CrossRef]
70. Zhang, Y.-C.; Si, D.-K.; Zhao, B. The Convergence of Sulphur Dioxide (SO_2) Emissions Per Capita in China. *Sustainability* **2020**, *12*, 1781. [CrossRef]

71. Cheng, B.; Dai, H.; Wang, P.; Xie, Y.; Chen, L.; Zhao, D.; Masui, T. Impacts of low-carbon power policy on carbon mitigation in Guangdong Province, China. *Energy Policy* **2016**, *88*, 515–527. [CrossRef]
72. Li, W.; Xiang, B.; Zhang, R.; Li, G.; Wang, Z.; Su, B.; Eric, T.M. Impact of Resource-Based Economic Transformation Policy on Sulfur Dioxide Emissions: A Case Study of Shanxi Province. *Sustainability* **2022**, *14*, 8253. [CrossRef]
73. Liu, H.; Zhong, Y.; Zhang, C. Energy Costs of Reducing Industrial Sulfur Dioxide Emissions in China. *Sustainability* **2021**, *13*, 10726. [CrossRef]
74. Altamira-Colado, E.; Cuevas-González, D.; Reyna, M.A.; García-Vázquez, J.P.; Avitia, R.L.; Osornio-Vargas, A.R. Drone-Assisted Particulate Matter Measurement in Air Monitoring: A Patent Review. *Atmosphere* **2024**, *15*, 515. [CrossRef]
75. Prikaz, M.; Fang, C.; Dash, S.; Wang, J. Origin and Background Estimation of Sulfur Dioxide in Ulaanbaatar, 2017. *Environments* **2018**, *5*, 136. [CrossRef]
76. Al-Hurban, A.; Khader, S.; Alsaber, A.; Pan, J. Air Quality Assessment in the State of Kuwait during 2012 to 2017. *Atmosphere* **2021**, *12*, 678. [CrossRef]
77. Liakakou, E.; Fourtziou, L.; Paraskevopoulou, D.; Speyer, O.; Lianou, M.; Grivas, G.; Myriokefalitakis, S.; Mihalopoulos, N. High-Resolution Measurements of SO_2, HNO_3 and HCl at the Urban Environment of Athens, Greece: Levels, Variability and Gas to Particle Partitioning. *Atmosphere* **2022**, *13*, 218. [CrossRef]
78. D'Amico, F.; Ammoscato, I.; Gullì, D.; Avolio, E.; Lo Feudo, T.; De Pino, M.; Cristofanelli, P.; Malacaria, L.; Parise, D.; Sinopoli, S.; et al. Integrated analysis of methane cycles and trends at the WMO/GAW station of Lamezia Terme (Calabria, Southern Italy). *Atmosphere* **2024**, *15*, 946. [CrossRef]
79. D'Amico, F.; Gullì, D.; Lo Feudo, T.; Ammoscato, I.; Avolio, E.; De Pino, M.; Cristofanelli, P.; Busetto, M.; Malacaria, L.; Parise, D.; et al. Cyclic and multi-year characterization of surface ozone at the WMO/GAW coastal station of Lamezia Terme (Calabria, Southern Italy): Implications for the local environment, cultural heritage, and human health. *Environments* **2024**, *11*, 227. [CrossRef]
80. Gattuso, D.; Pellicanò, D.; Cassone, G. Policies and Models for Efficient and Eco-sustainable Ports. *Open Transplant. J.* **2023**, *17*, e26671212265181. [CrossRef]
81. Weibring, P.; Swartling, J.; Edner, H.; Svanberg, S.; Caltabiano, T.; Condarelli, D.; Cecchi, G.; Pantani, L. Optical monitoring of volcanic sulphur dioxide emissions–comparison between four different remote-sensing spectroscopic techniques. *Opt. Lasers Eng.* **2002**, *37*, 267–284. [CrossRef]
82. Haulet, R.; Zettwoog, P.; Sabroux, J. Sulphur dioxide discharge from Mount Etna. *Nature* **1977**, *268*, 715–717. [CrossRef]
83. Malinconico, L. Fluctuations in SO_2 emission during recent eruptions of Etna. *Nature* **1979**, *278*, 43–45. [CrossRef]
84. Jaeschke, W.; Berresheim, H.; Georgii, H.-W. Sulfur emissions from Mt. Etna. *J. Geophys. Res.-Oceans* **1982**, *87*, 7253–7261. [CrossRef]
85. Salerno, G.G.; Burton, M.R.; Oppenheimer, C.; Caltabiano, T.; Randazzo, D.; Bruno, N.; Longo, V. Three-years of SO_2 flux measurements of Mt. Etna using an automated UV scanner array: Comparison with conventional traverses and uncertainties in flux retrieval. *J. Volcanol. Geotherm. Res.* **2009**, *183*, 76–83. [CrossRef]
86. de Ronde, C.E.J.; Massoth, G.J.; Baker, E.T.; Lupton, J.E. Submarine hydrothermal venting related to volcanic arcs. In *Volcanic, Geothermal, and Ore-Forming Fluids*; Simmons, S.F., Graham, I.J., Eds.; Giggenbach Memorial Volume; The Society of Economic Geologists: Littleton, CO, USA, 2003; Volume 10, pp. 91–110.
87. Allard, P.; Carbonnelle, J.; Métrich, N.; Loyer, H.; Zettwoog, P. Sulphur output and magma degassing budget of Stromboli volcano. *Nature* **1994**, *368*, 326–330. [CrossRef]
88. Barnie, T.; Bombrun, M.; Burton, M.R.; Harris, A.; Sawyer, G. Quantification of gas and solid emissions during Strombolian explosions using simultaneous sulphur dioxide and infrared camera observations. *J. Volcanol. Geotherm. Res.* **2015**, *300*, 167–174. [CrossRef]
89. McGonigle, A.J.S.; Oppenheimer, C.; Hayes, A.R.; Galle, B.; Edmonds, M.; Caltabiano, T.; Salerno, G.; Burton, M.; Mather, T.A. Suplhur dioxide fluxes from Mount Etna, Vulcano, and Stromboli measured with an automated scanning ultraviolet spectrometer. *J. Geophys. Res.-Solid. Earth* **2003**, *108*, 2455. [CrossRef]
90. Aiuppa, A.; Inguaggiato, S.; McGonigle, A.J.S.; O'Dwyer, M.; Oppenheimer, C.; Padgett, M.J.; Rouwet, D.; Valenza, M. H2S fluxes from Mt. Etna, Stromboli, and Vulcano (Italy) and implication for the sulfur budget at volcanoes. *Geochim. Cosmochim. Acta* **2005**, *69*, 1861–1871. [CrossRef]
91. D'Alessandro, W.; Aiuppa, A.; Bellomo, S.; Brusca, L.; Calabrese, S.; Kyriakopoulos, K.; Liotta, M.; Longo, M. Sulphur-gas concentrations in volcanic and geothermal areas in Italy and Greece: Characterising potential human exposures and risks. *J. Geochem. Explor.* **2013**, *131*, 1–13. [CrossRef]
92. Gurrieri, S.; Liuzzo, M.; Giuffrida, G.; Boudoire, G. The first observations of CO_2 and CO_2/SO_2 degassing variations recorded at Mt. Etna during the 2018 eruptions followed by three strong earthquakes. *Ital. J. Geosci.* **2021**, *140*, 95–106. [CrossRef]

93. Cristofanelli, P.; Busetto, M.; Calzolari, F.; Ammoscato, I.; Gullì, D.; Dinoi, A.; Calidonna, C.R.; Contini, D.; Sferlazzo, D.; Di Iorio, T.; et al. Investigation of reactive gases and methane variability in the coastal boundary layer of the central Mediterranean basin. *Elem. Sci. Anth.* **2017**, *5*, 12. [CrossRef]
94. D'Amico, F.; Ammoscato, I.; Gullì, D.; Avolio, E.; Lo Feudo, T.; De Pino, M.; Cristofanelli, P.; Malacaria, L.; Parise, D.; Sinopoli, S.; et al. Trends in CO, CO_2, CH_4, BC, and NO_x during the first 2020 COVID-19 lockdown: Source insights from the WMO/GAW station of Lamezia Terme (Calabria, Southern Italy). *Sustainability* **2024**, *16*, 8229. [CrossRef]
95. Federico, S.; Pasqualoni, L.; Sempreviva, A.M.; De Leo, L.; Avolio, E.; Calidonna, C.R.; Bellecci, C. The seasonal characteristics of the breeze circulation at a coastal Mediterranean site in South Italy. *Adv. Sci. Res.* **2010**, *4*, 47–56. [CrossRef]
96. Federico, S.; Pasqualoni, L.; De Leo, L.; Bellecci, C. A study of the breeze circulation during summer and fall 2008 in Calabria, Italy. *Atmos. Res.* **2010**, *97*, 1–13. [CrossRef]
97. NOAA National Geophysical Data Center. ETOPO1 1 Arc-Minute Global Relief Model. NOAA National Centers for Environmental Information. 2009. Available online: https://www.ncei.noaa.gov/access/metadata/landing-page/bin/iso?id=gov.noaa.ngdc.mgg.dem:316 (accessed on 13 November 2024).
98. Amante, C.; Eakins, B.W. *ETOPO1 1 Arc-Minute Global Relief Model: Procedures, Data Sources and Analysis. NOAA Technical Memorandum NESDIS NGDC-24*; National Geophysical Data Center: Boulder, CO, USA, 2009. [CrossRef]
99. European Commission. European Marine Observation and Data Network (EMODnet). Available online: https://emodnet.ec.europa.eu/en/bathymetry (accessed on 13 November 2024).
100. D'Amico, F.; Ammoscato, I.; Gullì, D.; Avolio, E.; Lo Feudo, T.; De Pino, M.; Cristofanelli, P.; Malacaria, L.; Parise, D.; Sinopoli, S.; et al. Anthropic-induced variability of greenhouse gasses and aerosols at the WMO/GAW coastal site of Lamezia Terme (Calabria, Southern Italy): Towards a new method to assess the weekly distribution of gathered data. *Sustainability* **2024**, *16*, 8175. [CrossRef]
101. Gullì, D.; Avolio, E.; Calidonna, C.R.; Lo Feudo, T.; Torcasio, R.C.; Sempreviva, A.M. Two years of wind-lidar measurements at an Italian Mediterranean Coastal Site. In European Geosciences Union General Assembly 2017, EGU–Division Energy, Resources & Environment, ERE. *Energy Procedia* **2017**, *125*, 214–220. [CrossRef]
102. Avolio, E.; Federico, S.; Miglietta, M.M.; Lo Feudo, T.; Calidonna, C.R.; Sempreviva, A.M. Sensitivity analysis of WRF model PBL schemes in simulating boundary-layer variables in southern Italy: An experimental campaign. *Atmos. Res.* **2017**, *192*, 58–71. [CrossRef]
103. Lo Feudo, T.; Calidonna, C.R.; Avolio, E.; Sempreviva, A.M. Study of the Vertical Structure of the Coastal Boundary Layer Integrating Surface Measurements and Ground-Based Remote Sensing. *Sensors* **2020**, *20*, 6516. [CrossRef]
104. D'Amico, F.; Calidonna, C.R.; Ammoscato, I.; Gullì, D.; Malacaria, L.; Sinopoli, S.; De Benedetto, G.; Lo Feudo, T. Peplospheric influences on local greenhouse gas and aerosol variability at the Lamezia Terme WMO/GAW regional station in Calabria, Southern Italy: A multiparameter investigation. *Sustainability* **2024**, *16*, 10175. [CrossRef]
105. Malacaria, L.; Parise, D.; Lo Feudo, T.; Avolio, E.; Ammoscato, I.; Gullì, D.; Sinopoli, S.; Cristofanelli, P.; De Pino, M.; D'Amico, F.; et al. Multiparameter detection of summer open fire emissions: The case study of GAW regional observatory of Lamezia Terme (Southern Italy). *Fire* **2024**, *7*, 198. [CrossRef]
106. D'Amico, F.; De Benedetto, G.; Malacaria, L.; Sinopoli, S.; Calidonna, C.R.; Gullì, D.; Ammoscato, I.; Lo Feudo, T. Tropospheric and surface measurements of combustion tracers during the 2021 Mediterranean wildfire crisis: Insights from the WMO/GAW site of Lamezia Terme in Calabria, Southern Italy. *Under review*.
107. Calidonna, C.R.; Avolio, E.; Gullì, D.; Ammoscato, I.; De Pino, M.; Donateo, A.; Lo Feudo, T. Five Years of Dust Episodes at the Southern Italy GAW Regional Coastal Mediterranean Observatory: Multisensors and Modeling Analysis. *Atmosphere* **2020**, *11*, 456. [CrossRef]
108. Veefkind, J.P.; Aben, I.; McMullan, K.; Forster, H.; de Vries, J.; Otter, G.; Claas, J.; Eskes, H.J.; de Haan, J.F.; Kleipool, Q.; et al. TROPOMI on the ESA Sentinel-5 Precursor: A GMES mission for global observations of the atmospheric composition for climate, air quality and ozone layer applications. *Remote Sens. Environ.* **2012**, *120*, 70–83. [CrossRef]
109. Romahn, F.; Pedergnana, M.; Loyola, D.; Apituley, A.; Sneep, M.; Veefkind, J.; Theys, N.; Hedelt, P. Sentinel-5 Precursor/TROPOMI Level 2 Product User Manual Sulphur Dioxide SO2, Sulphur Dioxide SO2. 2020. Available online: https://sentinel.esa.int/documents/247904/2474726/Sentinel-5P-Level-2-Product-User-Manual-Sulphur-Dioxide (accessed on 13 November 2024).
110. Theys, N.; De Smedt, I.; Lerot, C.; Yu, H.; Van Roozendael, M. S5P/TROPOMI SO2 ATBD, BIRA-IASIB (Doc. No. S5PBIRA-L2-400EATBD). 2022. Available online: https://sentinels.copernicus.eu/documents/247904/2476257/Sentinel-5P-ATBD-SO2-TROPOMI (accessed on 13 November 2024).
111. *Copernicus Sentinel-5P (Processed by ESA), 2020, TROPOMI Level 2 Sulphur Dioxide Total Column, Version 02*; European Space Agency: Paris, France, 2020. [CrossRef]
112. Apituley, A.; Pedergnana, M.; Sneep, M.; Veefkind, J.P.; Loyola, D.H.O. *Sentinel-5 Precursor/TROPOMI Level 2 Product User Manual Methane*; Royal Netherlands Meteorological Institute: De Bilt, The Netherlands, 2022.

113. Barrese, E.; Valentini, M.; Scarpelli, M.; Samele, P.; Malacaria, L.; D'Amico, F.; Lo Feudo, T. Assessment of formaldehyde's impact on indoor environments and human health via the integration of satellite tropospheric total columns and outdoor ground sensors. *Sustainability* **2024**, *16*, 9669. [CrossRef]
114. Earth Observation Center. *Sentinel-5P TROPOMI L3 Data ©DLR for 2020*; Earth Observation Center: Hatoyama, Japan, 2024; Available online: https://geoservice.dlr.de/data-assets/ozxr4ngp0473.html (accessed on 10 January 2025). [CrossRef]
115. Theys, N.; Fioletov, V.; Li, C.; De Smedt, I.; Lerot, C.; McLinden, C.; Krotkov, N.; Griffin, D.; Clarisse, L.; Hedelt, P.; et al. A sulfur dioxide Covariance-Based Retrieval Algorithm (COBRA): Application to TROPOMI reveals new emission sources. *Atmos. Chem. Phys.* **2021**, *21*, 16727–16744. [CrossRef]
116. Theys, N.; De Smedt, I.; Yu, H.; Danckaert, T.; van Gent, J.; Hörmann, C.; Wagner, T.; Hedelt, P.; Bauer, H.; Romahn, F.; et al. Sulfur dioxide retrievals from TROPOMI onboard Sentinel-5 Precursor: Algorithm Theoretical Basis. *Atmos. Meas. Tech.* **2017**, *10*, 119–153. [CrossRef]
117. Spearman, C. The Proof and Measurement of Association between Two Things. *Am. J. Psychol.* **1904**, *15*, 72–101. [CrossRef]
118. Schober, P.; Boer, C.; Schwarte, L.A. Correlation Coefficients: Appropriate Use and Interpretation. *Anesth. Analg.* **2018**, *126*, 1763–1768. [CrossRef]
119. Myers, J.L.; Well, A.D.; Lorch, R.F., Jr. *Research Design and Statistical Analysis*, 3rd ed.; Routledge: New York, NY, USA, 2010; p. 832. [CrossRef]
120. Gerasopoulos, E.; Kouvarakis, G.; Vrekoussis, M.; Donoussis, C.; Mihalopoulos, N.; Kanakidou, M. Photochemical ozone production in the Eastern Mediterranean. *Atmos. Environ.* **2006**, *40*, 3057–3069. [CrossRef]
121. Kalabokas, P.D.; Mihalopoulos, N.; Ellul, R.; Kleanthous, S.; Repapis, C.C. An investigation of the meteorological and photochemical factors influencing the background rural and marine surface ozone levels in the Central and Eastern Mediterranean. *Atmos. Environ.* **2008**, *42*, 7894–7906. [CrossRef]
122. Monks, P.S.; Granier, C.; Fuzzi, S.; Stohl, A.; Williams, M.L.; Akimoto, H.; Amann, M.; Baklanov, A.; Baltensperger, U.; Bey, I.; et al. Atmospheric composition change—Global and regional air quality. *Atmos. Environ.* **2009**, *43*, 5268–5350. [CrossRef]
123. Lelieveld, J.; Berresheim, H.; Borrmann, S.; Crutzen, P.J.; Dentener, F.J.; Fischer, H.; Feichter, J.; Flatau, P.J.; Heland, J.; Holzinger, R.; et al. Global Air Pollution Crossroads over the Mediterranean. *Science* **2002**, *298*, 794–799. [CrossRef]
124. Henne, S.; Furger, M.; Nyeki, S.; Steinbacher, M.; Neininger, B.; de Wekker, S.F.J.; Dommen, J.; Spichtinger, N.; Stohl, A.; Prévôt, A.S.H. Quantification of topographic venting of boundary layer air to the free troposphere. *Atmos. Chem. Phys.* **2004**, *4*, 497–509. [CrossRef]
125. Duncan, B.N.; West, J.J.; Yoshida, Y.; Fiore, A.M.; Ziemke, J.R. The influence of European pollution on ozone in the Near East and northern Africa. *Atmos. Chem. Phys.* **2008**, *8*, 2267–2283. [CrossRef]
126. Grandin, R.; Boichu, M.; Mathurin, T.; Pascal, N. Automatic estimation of daily volcanic sulfur dioxide gas flux from TROPOMI satellite observations: Application to Etna and Piton de la Fournaise. *J. Geophys. Res.-Solid. Earth* **2024**, *129*, e2024JB029309. [CrossRef]
127. Calidonna, C.R.; D'Amico, F.; Ammoscato, I.; Malacaria, L.; Gulli, D.; Lo Feudo, T.; Sinopoli, S.; De Benedetto, G.; Mona, L.; Dema, C.; et al. Continuous δ13C-CO2 and δ13C-CH4 Measurements in the Atmosphere—Data Gathered at Lamezia Terme (Calabria, Southern Italy) Between July and 24. Version 1. Available online: https://hub.itineris.cnr.it/datasets/ (accessed on 10 January 2025). [CrossRef]
128. Rizzo, A.L.; Liuzzo, M.; Ancellin, M.A.; Jost, H.J. Real-time measurements of $\delta^{13}C$, CO_2 concentration, and CO_2/SO_2 in volcanic plume gases at Mount Etna, Italy, over 5 consecutive days. *Chem. Geol.* **2015**, *411*, 182–191. [CrossRef]
129. Fischer, T.P.; Lopez, T.M. First airborne samples of a volcanic plume for $\delta^{13}C$ of CO_2 determinations. *Geophys. Res. Lett.* **2016**, *43*, 3272–3279. [CrossRef]
130. Boudoire, G.; Grassa, F.; Giuffrida, G.; Liuzzo, M. Recommendations and protocols for the sue of the isotope ratio infrared spectrometer (Delta Ray) to measure stable isotopes from CO_2: An application to volcanic emissions at Mount Etna and Stromboli (Sicily, Italy). *Geofluids* **2020**, *2020*, 4598190. [CrossRef]
131. Di Martino, R.M.R.; Gurrieri, S. Quantification of the Volcanic Carbon Dioxide in the Air of Vulcano Porto by Stable Isotope Surveys. *J. Geophys. Res.–Atmos.* **2022**, *128*, e2022JD037706. [CrossRef]
132. Ashbaugh, L.L.; Malm, W.C.; Sadeh, W.Z. A residence time probability analysis of sulfur concentrations at grand Canyon National Park. *Atmos. Environ.* **1985**, *19*, 1263–1270. [CrossRef]
133. Gao, N.; Cheng, M.-D.; Hopke, P.K. Potential source contribution function analysis and source apportionment of sulfur species measured at Rubidoux, CA during the Southern California Air Quality Study, 1987. *Anal. Chim. Acta* **1993**, *277*, 369–380. [CrossRef]
134. Biegalski, S.R.; Hopke, P.K. Total potential source contribution function analysis of trace elements determined in aerosol samples collected near Lake Huron. *Environ. Sci. Technol.* **2004**, *38*, 4276–4284. [CrossRef]
135. Hsu, Y.-K.; Holsen, T.M.; Hopke, P.K. Comparison of hybrid receptor models to locate PCB sources in Chicago. *Atmos. Environ.* **2003**, *37*, 545–562. [CrossRef]

136. Brereton, C.A.; Johnson, M.R. Identifying sources of fugitive emissions in industrial facilities using trajectory statistical methods. *Atmos. Environ.* **2012**, *51*, 46–55. [CrossRef]
137. Cheng, I.; Zhang, L.; Blanchard, P.; Dalziel, J.; Tordon, R. Concentration-weighted trajectory approach to identifying potential sources of speciated atmospheric mercury at an urban coastal site in Nova Scotia, Canada. *Atmos. Chem. Phys.* **2013**, *13*, 6031–6048. [CrossRef]
138. Dimitriou, K. The Dependence of PM Size Distribution from Meteorology and Local-Regional Contributions, in Valencia (Spain)—A CWT Model Approach. *Aerosol Air Qual. Res.* **2015**, *15*, 1979–1989. [CrossRef]